

UNIVERSITY OF BREMEN

**The impacts of Arctic sea ice reduction on
the ocean circulation from global coupled
model simulations**

by

Camila Pinheiro Campos

A thesis submitted in partial fulfillment for the
degree of Master of Science

in the

Institute of Environmental Physics

Alfred Wegener Institute Helmholtz Centre for Polar and Marine Research

August 12, 2015

Author: Camila Pinheiro Campos

Matriculation number: 2953375

Supervisor: Prof. Dr. Thomas Jung

Second examiner: Prof Dr. Torsten Kanzow

Declaration of Authorship

- Hereby I assure that my Master Thesis is a result of my personal work, and that I did not rely on any further sources or means besides as indicated by me.
- All passages literally or in a general manner obtained from published sources are cited as such.
- The Master Thesis must not be altered once handed in.

Signature:

Date:

Erklärung zur Autorschaft

Urheberrechtliche Erklärung Erklärung gem. § 10 (10) Allgemeiner Teil der MPO vom
27.10.2010

- Hiermit versichere ich, dass ich meine Masterarbeit ohne fremde Hilfe angefertigt habe, und dass ich keine anderen als die von mir angegebenen Quellen und Hilfsmittel benutzt habe.
- Alle Stellen, die wörtlich oder sinngemäß aus Veröffentlichungen entnommen sind, habe ich unter Angabe der Quellen als solche kenntlich gemacht.
- Die Masterarbeit darf nach Abgabe nicht mehr verändert werden.

Unterschrift:

Datum:

UNIVERSITY OF BREMEN

Abstract

Institute of Environmental Physics

Alfred Wegener Institute Helmholtz Centre for Polar and Marine Research

Master of Science

by [Camila Pinheiro Campos](#)

The sensitivity of Arctic Ocean to a gradual sea ice decline is addressed by using the global coupled model ECHAM6-FESOM we address. Sea ice retraction is forced by different perturbations in three idealized numerical experiments (*I*) reduced albedo, *II*) reduced lead closing parameter, *III*) added longwave). Results are compared against a reference run. It is shown that over long time scales ocean responses establish comparably in all sensitivity experiments. A sequence of mechanical and dynamical feedbacks takes place and lead to enhanced circulation of the anticyclonic Beaufort Gyre and Transpolar Drift. Consequently, increased export of meltwater through the Fram Strait sets in and, as a compensation effect, augmented volume flux of Atlantic Water into the Barents Sea occurs. Altogether, the "Atlantification" of the Barents Sea occurs concurrently to changes in local ocean circulation. Anomalously high heat transport to the Barents Sea is caused mainly due to the warming of waters upstream. The anomalous heat inflow enlarges local heat loss from the ocean to the atmosphere, and contributes to warming of the atmosphere. The heat not passed to the atmosphere is carried within the Arctic intermediate layer, and may eventually have impact on crucial regions beyond the limits of the Arctic Ocean.

Acknowledgements

I take this opportunity to reach my sincere gratitude and appreciation to all those who made this Master thesis possible.

First of all, I would like to thank Prof. Dr. Thomas Jung for accepting me as a Master student in the Climate Dynamics group at the Alfred Wegener Institute. I am very grateful for the opportunity of working with such an exciting topic. His inspiring suggestions and enthusiasm have been very important for the development of this thesis content.

My deepest gratitude also goes to Dr. Tido Semmler, for the constant help, encouragement and highly valuable input since being one of my thesis examiners from the very beginning. I have been very fortunate to have a mentor who has allowed me so much independence and at the same time prompt guidance whenever it was needed. I am also thankful to him for the revisions of this manuscript.

I thank all the colleagues from the Climate Dynamics group for constructive suggestions and comments on this work. Furthermore, I thank Prof. Dr. Torsten Kanzow for the important discussion and ideas shared at a crucial moment, and for examining my thesis.

I would like to acknowledge the PEP staff for supporting me from the beginning of the postgraduate program.

To my friends in Germany and those scattered around the world, I am thankful for making life so interesting and happy.

Finally, I would like to thank my family. I wish to thank Mathias, my best friend and husband, for the inspiring patience, everlasting positive attitude and caring support. Thank you for all the exciting and inspiring discussions, and also for the unique restorative moments of silence. I would like to express my sincerest gratitude to my mother, father and brother. I would not have been able to achieve so much happiness in my life without their unconditional love and support. Despite the geographical distance, they have always made sure I felt their encouragement and constant inspiration, always motivating me to chase new challenges.

Contents

Declaration of Authorship	iv
Erklärung zur Autorschaft	v
Abstract	vi
Acknowledgements	vii
List of Figures	xi
List of Tables	xiii
Abbreviations and Units	xv
1 Introduction	1
1.1 Sea Ice	2
1.1.1 Seasonal cycle	2
1.1.2 Importance in the Climate System	3
1.1.3 Arctic Sea Ice in a Changing Climate	5
1.2 Arctic Water Masses and Circulation	6
1.3 Atlantic Gateways	9
1.3.1 Fram Strait	9
1.3.2 Barents Sea	10
1.4 Arctic Ocean and the Atlantic Meridional Overturning Circulation	11
1.5 Research Question	13
1.6 Approach	14
2 Method	15
2.1 Model and Experimental Setup	15
2.2 ECHAM	16
2.3 FESOM	16
2.4 Sensitivity Simulations Setup	16
2.4.1 Added Longwave radiation experiment [LW]	18
2.4.2 Reduced Albedo [ALB]	18
2.4.3 Lead Closing Parameter [LEAD]	19

2.5	Output Evaluation	20
3	Results and Discussion	23
3.1	Sea ice	23
3.2	Atmosphere	32
3.3	Arctic Ocean Circulation	34
3.3.1	Hydrography	34
3.3.2	Volume and Heat fluxes	38
3.3.2.1	Fram Strait: Volume Transport out of the Arctic	40
3.3.2.2	Barents Sea: Volume and Heat Transport into the Arctic	44
4	Summary and Outlook	51
4.1	Summary	51
4.2	Outlook	53
A	Glossary	55
B	Figures	57
C	Tables	65
	Bibliography	69

List of Figures

1.1	September sea ice extent decline trend from NSIDC	5
1.2	Vertical profile of temperature across the Arctic Ocean	6
1.3	Arctic Ocean Temperature-Salinity (TS) diagram	7
1.4	Surface and intermediate Arctic Ocean circulation schemes	8
1.5	Barents Sea circulation scheme	12
2.1	ECHAM-FESOM mesh representation	15
2.2	FESOM 2D and 3D grid illustration	17
2.3	Scheme of REF and SENS simulations	17
2.4	Scheme of lead closing parameter	19
3.1	Comparison reference run with observation: sea ice area and sea ice volume	24
3.2	Average reference run (REF) 30-year sea ice concentration (SIC)	25
3.3	Climatological sea ice extent from NSIDC	25
3.4	Sea ice area time series for all experiments	26
3.5	Sea ice volume time series.	26
3.6	Sea ice area and sea ice volume 30-year climatology	28
3.7	Sea ice thickness: 150 year absolute values (REF) and difference maps (SENS - REF)	29
3.8	Sea ice concentration: 150 year absolute average (REF) and difference maps (SENS - REF)	30
3.9	Feedback loops	31
3.10	Sea surface temperature maps: absolute value (REF) and difference maps (SENS - REF)	36
3.11	Sea surface salinity maps: absolute value (REF) and difference maps (SENS - REF)	37
3.12	Sea surface height maps: absolute value (REF) and difference maps (SENS - REF)	39
3.13	Velocity across Fram Strait section: absolute value (REF) and difference maps (SENS - REF)	42
3.14	Salinity across Fram Strait section: absolute value (REF) and difference maps (SENS - REF)	43
3.15	Volume and Heat fluxes in the Barents Sea	45
3.16	Density averaged over 230 – 680m in the Barents Sea: absolute value (REF) and difference maps (SENS - REF)	49
B.1	(SENS-2) Sea ice area and sea ice volume 30-year climatology	57

B.2	(SENS-2) Sea ice thickness: 150 year absolute values (REF) and difference maps (SENS - REF)	58
B.3	(SENS-2)Sea ice concentration: 150 year absolute average (REF) and difference maps (SENS - REF)	59
B.4	(SENS-2) Sea surface temperature maps: absolute value (REF) and difference maps (SENS - REF)	60
B.5	(SENS-2) Sea surface salinity maps: absolute value (REF) and difference maps (SENS - REF)	60
B.6	(SENS-2) Sea surface height maps: absolute value (REF) and difference maps (SENS - REF)	61
B.7	North Atlantic average 0 - 50 m ocean temperature maps: absolute value (REF) and difference plots (SENS-1)	61
B.8	(SENS-2) Velocity across Fram Strait section: absolute value (REF) and difference maps (SENS - REF)	62
B.9	(SENS-2) Salinity across Fram Strait section: absolute value (REF) and difference maps (SENS - REF)	62
B.10	(SENS-2) Density averaged over 230 – 680m in the Barents Sea: absolute value (REF) and difference maps (SENS - REF)	63

List of Tables

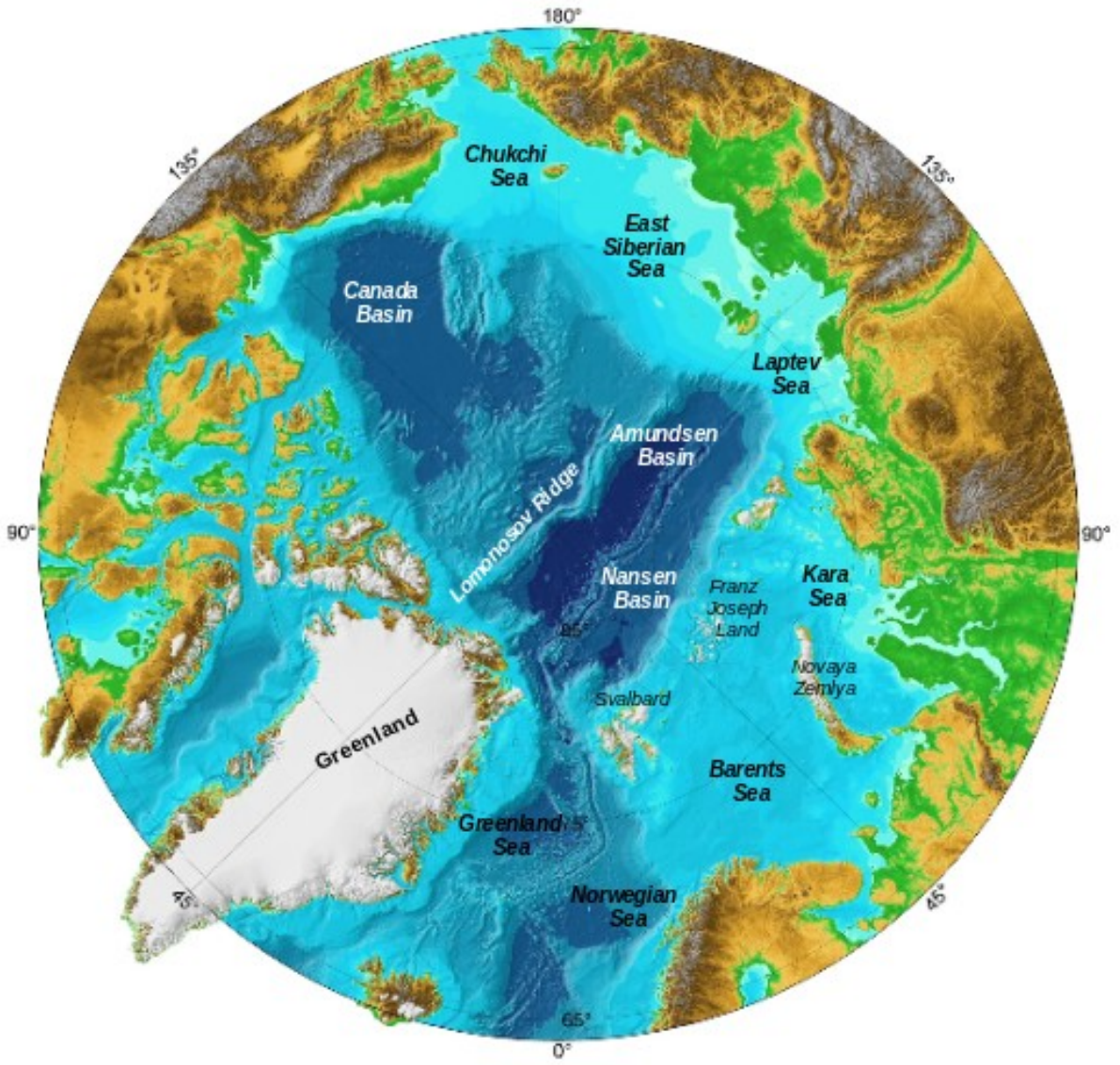
2.1	Lead closing parameter range of values for reference (REF) and sensitivity (LEAD) runs	20
3.1	Sea ice volume average reduction	28
3.2	Turbulent Heat Flux over Barents Sea	34
3.3	Averaged net Volume Flux changes through Fram Strait section	41
3.4	Averaged net Volume Flux changes through Barents Sea Entrance section	44
C.2	Ocean Heat Flux through BSE section	65
C.1	Volume Flux across FS and BSE sections. Inflow and outflow always referenced to the Arctic Ocean	66
C.3	Ocean-Atmosphere: Heat Flux over Barents Sea (SENS-2)	67

Abbreviations and Units

AMOC	Atlantic Meridional Overturning Circulation
AOGCM	Atmosphere Ocean Global Climate Model
AW	Atlantic Water
AWL	Atlantic Water Layer
BSE	Barents Sea Entrance
BSW	Barents Sea Water
BSX	Barents Sea EXit
CMIP	Coupled Model Intercomparison Project
CORE	Coordinated Ocean-Ice Reference Experiment
EGC	East Greenland Current
FESOM	Finite Element Sea-ice Ocean Model
GCM	Global Climate Model
GIN	Greenland Iceland Norwegian
KG	Kara Gate
LH	Latent Heat
LW	Longwave
MIZ	Marginal Ice Zone
NAC	North Atlantic Current
NwAC	Norwegian Atlantic Current
NADW	North Atlantic Deep Water
NAO	North Atlantic Oscillation
NH	Northern Hemisphere
NBS	Northern Barents Sea
PIOMAS	Pan Arctic Ocean Model Assimilation System
REF	Reference Simulation

SENS	Sensitivity Experiments
SH	Sensible Heat
SHem	Southern Hemisphere
SIA	Sea Ice Area
SIC	Sea Ice Concentration
SIT	Sea Ice Thickness
SIV	Sea Ice Volume
SSH	Sea Surface Height
SSS	Sea Surface Salinity
SST	Sea Surface Temperature
SW	Shortwave
WOA	World Ocean Atlas
WSC	West Spitsbergen Current

PSU	Practical Salinity Units
Sv	Sverdrups ($10^6 \text{ m}^3\text{s}^{-1}$)
TW	TeraWatts (10^{12} W)



Chapter 1

Introduction

The Arctic Ocean occupies only a small area of Earth's surface, and yet, it plays a crucial role in global energy and moisture budgets. Thus, the region strongly controls atmospheric and oceanographic circulations over high latitudes. Recently, it is undergoing severe environmental changes, and has been a hot topic among the climate scientific community ([Winton, 2008](#)).

A mean annual warming twice as fast as the global mean has been observed over the Arctic region. This process is referred to as *polar amplification* ([Winton, 2008](#)). One of the main indicators of the impacts of Arctic climate change is the sea ice cover. A drastic reduction of sea ice extent¹, sea ice thickness and length of ice season has been observed over the last three decades ([NSIDC, 2014](#); [IPCC, 2013](#)). The understanding of these changes, their triggers and consequences, has become a hot topic among the climate scientific community.

Because of its important role in determining high latitude and large scale atmospheric circulation, studies relying on Global Circulation Models (GCMs) have addressed impacts of Arctic sea ice on the atmosphere over regional scales and its teleconnections ([Bader et al., 2011](#); [Budikova, 2009](#); [Semmler et al., 2012](#)). [Bader et al. \(2011\)](#) conclude that sea ice conditions over the Arctic are key drivers of a large scale atmospheric mode, the North Atlantic Oscillation (NAO)². Accordingly, sea ice loss may displace jet stream more to the South, and thus contribute to different storm and precipitation patterns over Europe.

¹ See Appendix A – Glossary for definition

² alternation of atmospheric mass with centres of action near the Icelandic low and the Azores high

Interactions among the natural components of climate system are not yet fully understood, and are one of the main sources of uncertainty in the attempts to explain current state and predict the effects of climate change. Notwithstanding that some model based studies have included the ocean component, the critical link between sea ice-ocean has been little addressed. A thorough investigation of such interrelations becomes increasingly important on a changing climate. Hereby, the main objective of this work is to investigate the effects of sea ice decline on the ocean circulation. Hence, to support the upcoming analysis a brief description of current sea ice state and background information on the Arctic Ocean circulation is provided.

1.1 Sea Ice

1.1.1 Seasonal cycle

The seasonal cycle of sea ice occurs as consequence of periodic changes of incident solar radiation over high latitudes of the northern hemisphere (NH) and the southern hemisphere (SHem). As the cold season arrives, atmospheric temperatures rapidly begin to drop. This leads to a downward directed thermal gradient, and a direct loss of sensible heat from the upper ocean to the atmosphere takes place.

Dynamical instability in the upper meters of the ocean is generated as a consequence of density change. This vertical mixing is maintained until a significant layer of the upper water column approaches homogeneous temperatures. Once the freezing temperature for ocean water is reached (*i.e.* -1.9°C) sea ice structures begin to form and a salty solution (brine) is rejected into the water.

The processes which will define the initial microstructure of sea ice depends on environmental conditions. In turbulent conditions small crystals are the first structures formed. In quiescent areas, on the other hand, freezing forms a more homogeneous thin layer. The rate with which sea ice forms has a reverse effect on the overall expulsion of brine: faster (slower) build up of ice means less (more) rejection of salt. As a result of this process, sea ice salinity varies from 2 to 7 psu³ (Thomas and Dieckmann, 2009).

³ By convention salinity is a unitless variable, however to keep consistency with model outputs practical salinity units (PSU) is reported in this work

After initial formation in fall, sea ice grows further through winter months and increases its vertical and horizontal extent, and can develop highly complex and variable macrostructures (*e.g.* ridges, melt ponds, leads, polynyas). The later are determinant in regulating the interaction between sea ice - ocean and atmosphere. Ridges, melt ponds and lead have a reverse relation with the surface albedo⁴ of the ice cover, and any perturbation can give rise to a positive feedback loop in which more heat is absorbed, more ice is melted, the albedo is reduced. Additionally, leads are crucial connections between the relatively warm ocean and the cold atmosphere and guarantee important heat and gas exchanges; they represent a small fraction of sea ice covered area, and are responsible for 50% of the oceanic heat loss (Thomas and Dieckmann, 2009).

By the end of the cold season (*i.e.* March (September) in NH (SHem)) sea ice extent has reached its maximum and with gradual insolation increase the melting phase takes place. If complete melt occurs, the area is characterized by one year ice. However, if a cover of sea ice remains until the end of the warm season (*i.e.* September (March) in NH (SHem)) a multiyear layer of sea ice is established. Over half of the Arctic sea ice is multiyear, and the average sea ice thickness ranges from 2 – 3 m (Thomas and Dieckmann, 2009).

1.1.2 Importance in the Climate System

Sea ice is a highly reflective surface, with an albedo ranging from 50 – 70%. This value may be even higher in the presence of snow cover. Thicker sea ice supports a greater layer of snow and this system can reflect up to 90% of sunlight. If anomalous warming takes place, more sea ice melts and as a consequence the albedo of polar areas decreases, leading to further warming and melting. The described processes are the so-called ice-albedo feedback mechanism and are assumed to be the reason of nonlinear changes over polar regions (Winton, 2008).

As ice melts, low reflectance oceanic surface underneath is exposed and readily absorbs solar shortwave radiation. This higher intake of energy results in warming of the ocean water. The increase of sensible heat content changes the current energy balance in the system, and gives rise to the positive feedback mechanism through which further sea ice melt takes place (Serreze and Barry, 2011).

⁴ See Appendix A – Glossary for definition

Moreover, sea ice acts as powerful insulator between ocean and atmosphere, and dampens heat, mass and momentum fluxes at this interface. The heat exchange with the atmosphere at high latitudes is dominantly from the warm ocean to the cold atmosphere. The reduction of sea ice allows an increased absorption of shortwave radiation by the ocean in summer. Once the heat content of the water is increased the thick ice melts and/or only a thinner layer of sea ice can be formed. Thinner ice is less strong, thus is more susceptible to fracturing. Such features allow important exchange of heat (mostly turbulent heat) between ocean and atmosphere. Additionally, thinner and fracture ice provides less drag, and momentum transfer is increased (from atmosphere to ocean, and from ocean and atmosphere to the sea ice).

Sea ice formation and melt are crucial processes for the local oceanic stratification and global oceanic circulation. Cold regions where sea ice is formed are responsible for creating deep water masses which are a crucial part of the global oceanic heat distribution system (*Conveyor Belt*). The injection of brine during sea ice formation induces deep convection motion due to densification of upper layer ocean water; in some regions densification due to heat loss is enough to trigger the deep convection.

On the other hand, sea ice constitutes a freshwater source. Any anomalous discharge of Arctic Ocean and ice melt water has the potential of hindering deep convection sites, by creating an stable surface layer of fresh water. In turn this may impact the overturning system and distribution of heat. Such an occurrence is described in the 1970's during the event known as "Great Salinity Anomaly" ([Mauritzen et al., 2013](#)).

Hence, sea ice modulates all interaction between ocean and atmosphere, namely heat, mass and momentum transports, and potentially gives rise to nonlinear changes over polar regions ([Winton, 2008](#)). It is worth pointing out, although with no further discussion, the key role sea ice plays sustaining the polar ecosystem. It not only serves as platform for top predator animals as polar bears and walrus, but it also houses autothropic⁵ communities which live underneath it.

⁵ See Appendix A – Glossary for definition

1.1.3 Arctic Sea Ice in a Changing Climate

Satellite passive microwave observations indicate that over the last three decades summer minimum sea ice extent over the Arctic has decreased by 40% (Figure 1.1) (Pistone et al., 2014). The observed rate of sea ice retraction during the last decades has occurred faster than previously predicted (Figure 1.1) (Serreze and Barry, 2011). According to IPCC (2013), the observed retraction has been *very likely*⁶ enhanced by anthropogenic greenhouse gas emissions. Moreover, changes in atmospheric and ocean dynamics drive year-to-year variability. The interplay of both forcings is responsible for the event of lowest sea ice cover observed in September 2012 (Parkinson and Comiso, 2013).

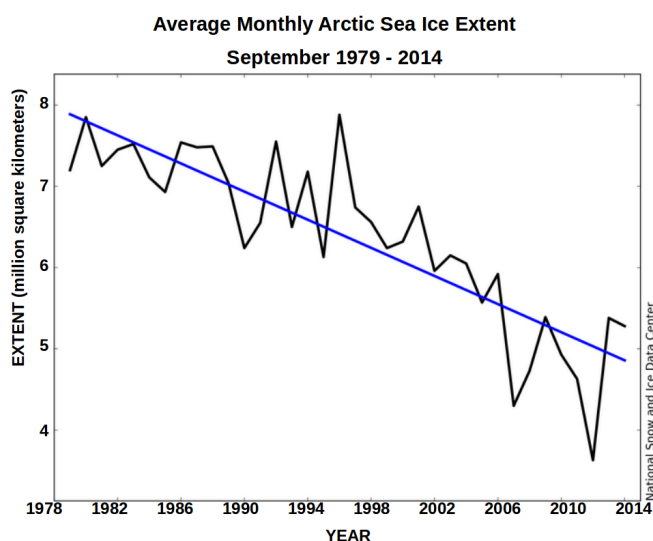


Figure 1.1: Climatological monthly average Arctic sea ice minimum (September) extent trend from 1979 to 2014. Image courtesy of the National Snow and Ice Data Center (NSIDC), University of Colorado, Boulder.

Pistone et al. (2014) report that observed changes in the mean August sea-ice zone albedo are -0.029 ± 0.011 per decade from 1982 - 2009. The reduction from 0.54 to 0.48 in the Arctic planetary albedo⁷ corresponds to additional $6.4 \pm 0.9 \text{ W/m}^2$ in the climate system. The decrease of sea ice is related to an increased latent heat flux from the ocean to the atmosphere. As a feedback response more condensation and cloud formation could be expected, which could compensate at least partly for the albedo loss at ocean surface. However, no significant increase in cloud cover has yet been observed (Pistone et al., 2014).

⁶ index define by the IPCC means *greater than 90 percent chance*

⁷ See Appendix A – Glossary for definition

Recent remote sensed measurements of sea ice thickness reveal that not only sea ice coverage has been decreasing, but also sea ice thickness: Arctic sea ice mean thickness changed from ca. 3m to approximately 1.5m between (Kwok et al., 2009). This indicates that from year to year more melt and less recovery is taking place. Changes in thickness of sea ice are inversely related to changes in shortwave radiation absorption by the ocean. According to IPCC (2013) it is *very likely* that the Arctic sea ice cover will continue shrinking and thinning year-round in the course of the 21st century as global mean surface temperature rises.

1.2 Arctic Water Masses and Circulation

The Arctic Ocean is connected to the surrounding seas through four main openings: Fram Strait, Barents Sea, Canadian Arctic Archipelago and Bering Strait (Figure 1.4 b). Due to this limited connection to the surrounding oceans, it can be also referred to as a mediterranean sea. According to this definition, ocean dynamics are determined by thermohaline gradients and modified by wind forcing (Tomczak and Godfrey, 1994). In this study we refer to the Greenland, Iceland and Norwegian (GIN) Seas and, eventually, the Labrador Sea as the Atlantic subarctic seas.

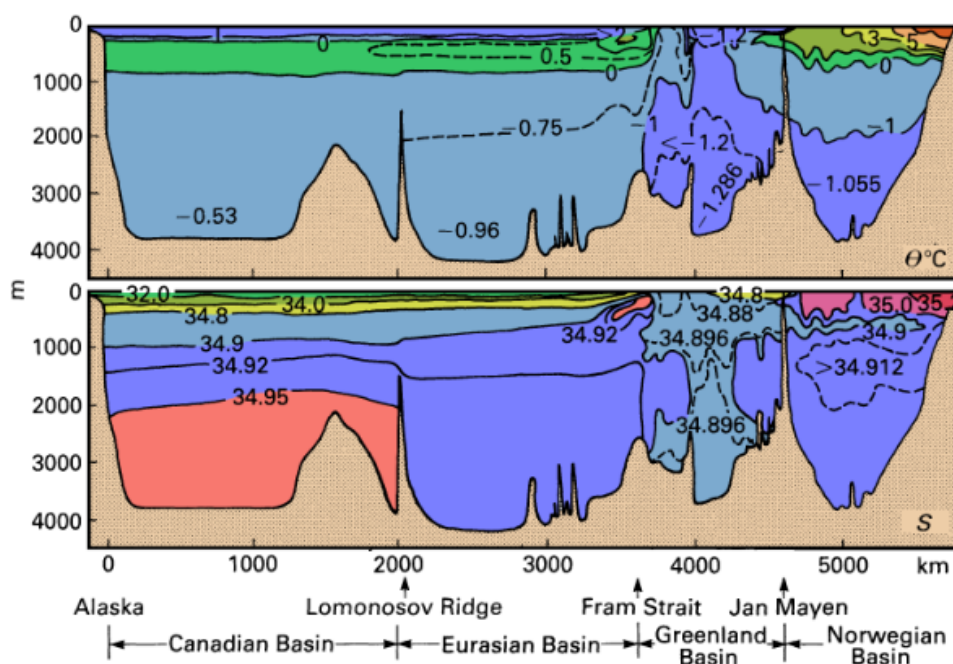


Figure 1.2: Stratification of water masses from the Norwegian Sea to the Canadian Basin. Reproduced from Tomczak and Godfrey (1994)

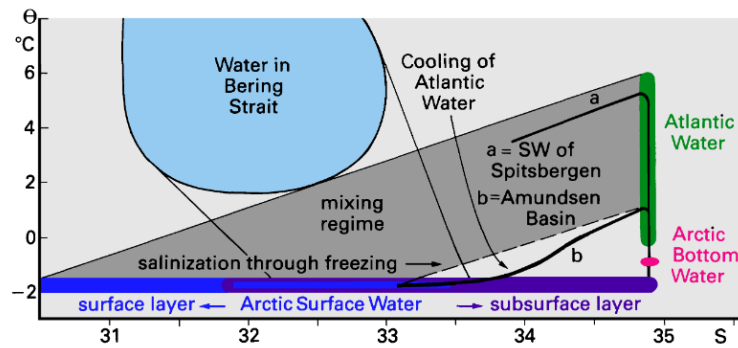


Figure 1.3: Temperature-Salinity (T-S) diagram for the Arctic Ocean water masses and two examples of station data (curves **a** and **b**). The hatched areas give T-S properties of source water masses; the thin lines limit the regions of all possible and observed T-S combinations produced by mixing. Cooling of Atlantic Water through mixing with Surface Water of the subsurface layer is indicated by the departure of the T-S curve from a straight mixing line in the Amundsen Basin. Reproduced from Tomczak and Godfrey (1994)

The stratification of water masses in the Arctic Ocean is shown in the scheme (Figure 1.2) from Tomczak and Godfrey (1994) as section that goes from the Norwegian Seas to the Canada Basin. Temperature and salinity of water masses are briefly described next and are depicted in the diagram shown in Figure 1.3.

The depth of the polar mixed layer varies according to wind forcing. It is characterized by water with temperature close to freezing point (-1.9°C), and has low content of salt. On a seasonal basis the variability of temperature and salinity on the upper layer is closely related to the seasonal sea ice cycle; that is, sea ice creates a fresher surface layer as it melts, and induces mixing of surface waters through brine rejection on freezing season.

The Pacific Water flowing through the Bering Strait is relatively warm and fresh ($T > 2^{\circ}\text{C}$ and $S < 33.0$ psu). This water is fundamentally confined to the upper layer 50 – 100 m over the western part of the Arctic basin. The Atlantic Water (AW), on the other contrary, is particularly important for the Arctic Ocean as a whole. The warm and saline ($T > 3^{\circ}\text{C}$ and $S > 34.8$ psu) water is provided by the Norwegian Atlantic Current (NwAC), flows through the Fram Strait and Barents Sea, and fills the intermediate depth of the Arctic Ocean, hereafter called the Atlantic Water Layer (AWL).

The intermediate layer (from below the pycnocline to approximately 1200 m) of the Arctic Ocean has temperatures up to several degrees above zero, ranging from 4°C in the vicinities of Atlantic inflow region, to $0 - 1^{\circ}\text{C}$ in the central Arctic Ocean, and

salinity greater than 34.8 psu. Below 2000m the basin is filled with the saline dense Arctic Deep Water. Due to bathymetric barriers (namely, Lomonosov Ridge) this water mass is confined to the Canadian Basin.

At the surface the circulation is characterized by the anticyclonic Beaufort Gyre in the Amerasian Basin, and a Transpolar Drift that transports the sea ice and surface water from shallow shelf seas (Chuckchi, East Siberian, Kara and Laptev) toward the Greenland Sea (Figure 1.4a). The proportion of this transport occurs accordingly to atmosphere and oceanic circulation regimes.

At intermediate depth the circulation is denoted by topographically driven cyclonic gyres (Figure 1.4b), which are substantially formed by waters flowing off the shelves and a large fraction of AW. The Lomonosov Ridge acts as a crucial topographic barrier for the exchange of waters between the Eurasian and Canadian basins.

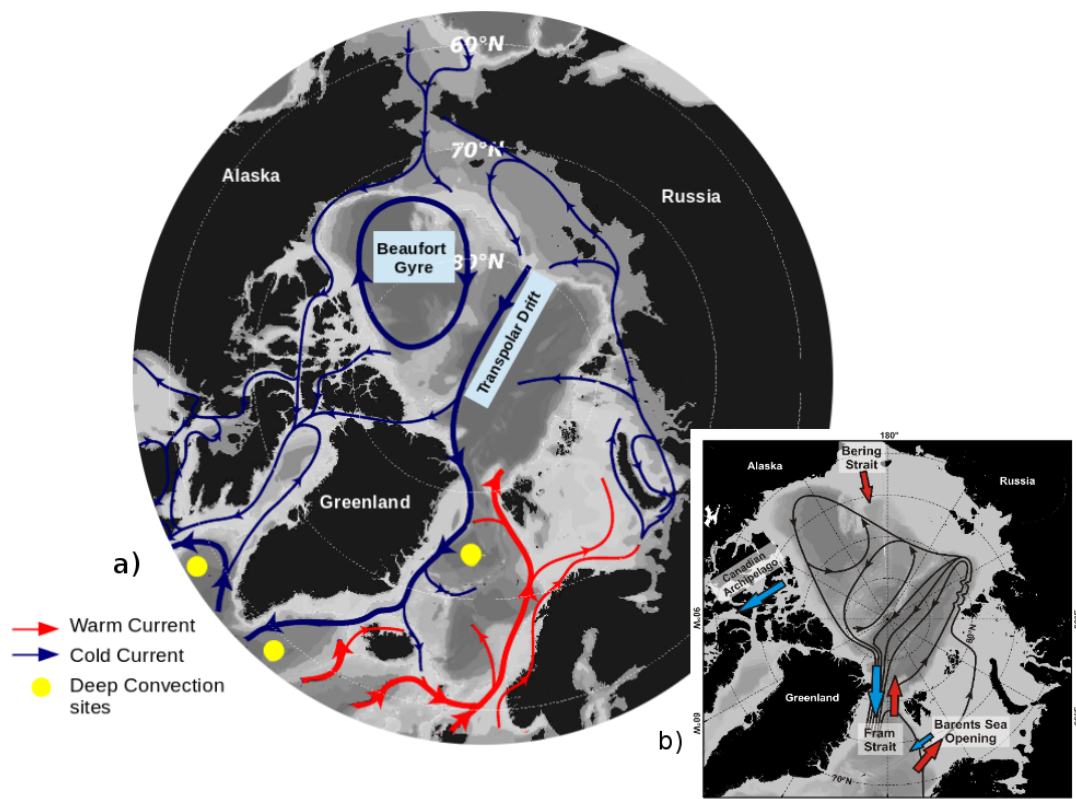


Figure 1.4: Arctic Ocean circulation scheme: **a)** indicates main surface warm (AW) and cold currents, and also key areas of deep convection, **b)** shows the circulation scheme of Atlantic-derived water and gateways to Atlantic and Pacific with a qualitative sketch of the flows through (reproduced from [Schauer and Beszczynska-Möller \(2009\)](#))

Intermediate and deep waters of the Arctic Ocean eventually exit through the Fram Strait, carried by the East Greenland Current (EGC). According to [Schauer et al. \(2008\)](#), the outflow of intermediate water originating in the Barents Sea takes place up to two decades later. The outflow is observed flowing along the Greenland continental slope and shelf.

The EGC transports water with an average temperature of $-1\text{ }^{\circ}\text{C}$ and salinity from 30 – 33 psu. In contrast, the AW carried by the NwAC has temperatures reaching up to $8\text{ }^{\circ}\text{C}$ and salinity 34 – 35 psu.

For the AW, temperature is the prevailing factor determining the water mass density. Nevertheless, thermal gradients in the polar oceans are small when compared to salinity, and for this reason, salinity is the leading driver of density changes within the Arctic Ocean.

1.3 Atlantic Gateways

To fulfill the scope of this work, the focus will be directed to the main connections of water to and from Atlantic Ocean. The Fram Strait and Barents Sea gateways play key role in the import of heat into the polar ocean along with sea ice export. The NwAC is fed by the warm and saline waters from the North Atlantic Current (NAC), and is the courier of the heat flowing through the openings. According to up-to-date estimates reviewed in [Beszczynska-Möller et al. \(2011\)](#) the net volume and heat fluxes through the Bering Strait are small when compared to those through Barents Sea: 0.8 Sv and 10 to 20⁸ TW, against 2.0 Sv and 50⁹ to 70¹⁰ TW. More information on water mass properties and circulation is provided next.

1.3.1 Fram Strait

The Fram Strait is a 500 km wide and 2,600 m deep passage located between Greenland and Svalbard. Due to its depth it configures as the only pathway of deep-water between the Arctic and the surrounding oceans. In addition, the Fram Strait is the

⁸ referenced to freezing temperature

⁹ referenced to $T_{ref}\ 0\text{ }^{\circ}\text{C}$

¹⁰ heat flux for closed volume budget

main region of sea ice export from the Arctic, mainly confined on the western part of this passage, where the EGC heads southward over the eastern Greenland continental slope.

Most of the sea ice carried by the EGC is transported across the Arctic Ocean from the eastern shallow shelf seas (Laptev and East Siberian Seas) by the Transpolar Drift. Hence, the Fram Strait plays an important role in regulating the amount of sea ice and freshwater within the Arctic ([Beszczynska-Möller et al., 2011](#)).

The warm and saline Atlantic Water inflow is limited to the eastern side of the strait as the West Spitsbergen Current (WSC). Its core is observed on the upper 500 m, but it fills the water column until further below. For this reason, along with the high velocities, the AW does not lose much heat to the atmosphere, preserving its warm temperature. A fraction of AW recirculates between 76°N and 78°N towards Greenland and the remaining part enters the Arctic Ocean and contributes to the AWL ([Walczowski, 2014](#)).

The easternmost branch interacts with sea ice in the vicinity of Svalbard and a less saline upper layer is created by ice melt. North of Svalbard this upper part is advected eastward together with the main Atlantic inflow as a boundary current along the Eurasian continental slope. The upper layer becomes stratified by ice melt in summer, and in winter the stability is disturbed by cooling, freezing and brine rejection down to the thermocline above the Atlantic layer ([Walczowski, 2014](#)).

1.3.2 Barents Sea

The Barents Sea covers 10% of the Arctic Ocean and has a mean depth of ca. 230 m. As a connection between the Arctic and the Atlantic Ocean it lays in a key area, where much of the heat transport takes place, both in ocean and atmosphere. The Barents Sea dominates the seasonal Arctic heat budget and has the most vigorous ocean-air exchange in the Arctic, which makes it a hot spot of influence on the high-latitude climate system. The inflow of AW to the Barents Sea accounts for about half of the northward heat transport to the Arctic Ocean and the Barents Sea combined ([Smedsrud et al., 2013](#)).

This shallow shelf sea is dominated by a cyclonic circulation as suggested in Figure 1.5. The AW fills the western part of the basin, and is separated from the cold and fresh Arctic Water ($T > 0^{\circ}\text{C}$ and $S < 34.7$ psu) by the polar fronts (Oziel et al., 2015).

The cooling and mixing of the Atlantic Waters, Arctic Waters and Norwegian Coastal Current Waters, is reinforced by brine rejections in winter and produces the dense Barents Sea Water (BSW).

A part of the BSW returns to the Norwegian Sea as cold, dense bottom water through the Bear Island Trough. The remaining BSW flows between Franz-Joseph-Land and Novaya Zemlya and can cascade down the St. Anna Trough into the Arctic Ocean forming 50% to 80% of the AWL (Schauer et al., 2002). Through this gateway the oceanic exchange is an order of magnitude larger than the one through the northern opening (between Svalbard and Franz-Joseph-Land) and the Kara Gate (Årthun et al., 2012; Smedsrud et al., 2013).

Lately, the Barents Sea plays an increasingly important role as a strong sink of anthropogenic carbon dioxide (CO_2) because of the combined effect of physical and biological pumps¹¹ (Smedsrud et al., 2013). Due to drift of warm AW, the region has a high biological production compared to other oceans of similar latitude. In fact, it accounts for 40% of the primary productivity of the whole Arctic. Local changes in ocean properties, circulation and sea ice cover could have significant influence on the biogeochemical feedbacks and marine ecosystem. Hence, the Barents Sea configures as a critical region of the Arctic Ocean.

1.4 Arctic Ocean and the Atlantic Meridional Overturning Circulation

The Arctic and Subarctic Oceans are key regions for the maintenance of the Atlantic branch of the meridional overturning circulation (AMOC), hosting crucial sites of deep water formation (included in Figure 1.4). Over lower latitude (Labrador Sea) densification is driven basically by air-sea thermal gradient / surface heat fluxes. Whereas further north (Irminger and Greenland Seas), deep convection occurs due

¹¹ See Appendix A – Glossary for definition

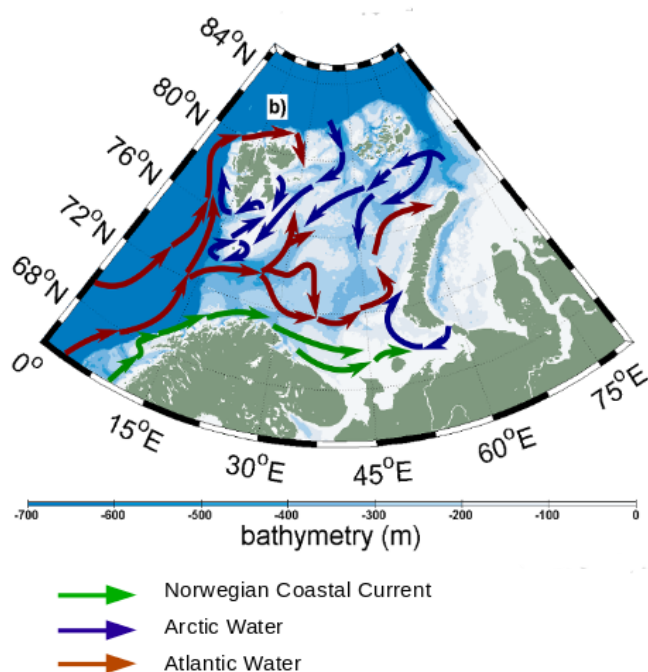


Figure 1.5: Barents Sea circulation scheme. Warm Atlantic Water in red. Blue arrows indicate cold and fresher water, and green arrows stand for diluted Atlantic water flowing as the Norwegian Coastal Current. Reproduced from [Oziel et al. \(2015\)](#)

to buoyancy fluxes controlled by brine rejection during sea ice formation. These waters sink to depth and spread as the North Atlantic Deep Water (NADW). Thereby a meridional density gradient between high and low latitudes is established ([Aagaard and Carmack, 1989](#)).

Changes in the sea ice state and deep ventilation of the Arctic Ocean may also reflect back on the AMOC. According to a review¹² by [Zickfeld et al. \(2007\)](#) the majority of researchers agree that changes in the freshwater and/or heat budget of the North Atlantic are most important in determining the future evolution of the AMOC. Moreover, the production of BSW determines the contribution of deep Arctic Water to the deep branches of the AMOC.

¹² Work based on interviews with 12 leading climate scientists about the possible effects of global climate change on the AMOC

1.5 Research Question

Recent observational studies report a warming of the North Atlantic Ocean with repercussions measured in the Arctic Ocean. [Holliday et al. \(2008\)](#) show since the 1990's temperature and salinity have rapidly increased in eastern North Atlantic subpolar gyre branch to the Fram Strait. According to [Schauer et al. \(2008\)](#), during the last decade a net temperature increase of the incoming AW in the Fram Strait of 1°C . Across the Barents Sea Opening, water mass temperature indicate an increase of 1°C over the period from 1997 - 2006 ([Beszczynska-Möller et al., 2011](#)). Accordingly, the warming of AW is accompanied by estimates of volume transport increase into the Barents Sea, setting a current "Atlantification" of the Barents Sea ([Oziel et al., 2015](#); [Smedsrud et al., 2013](#); [Årthun et al., 2012](#)).

Along with ocean warming Arctic sea ice is also undergoing severe change. While, it has been hypothesized that the inflow of warm AW into the Arctic Ocean has an influence on the decline and variability of sea ice extent and thickness ([Årthun et al., 2012](#); [Smedsrud et al., 2013](#); [Carmack et al., 2015](#)), [Itkin et al. \(2014\)](#) recently assessed the reverse relation, by addressing the question: what is the impact of sea ice reduction on the Arctic ocean circulation?

In the later work, idealized numerical simulation¹³, suggests that weaker sea ice gives rise to enhanced anticyclonic circulation of the Beaufort Gyre, and in contrast slows down the Transpolar Drift. Additionally, it was found a spread cooling of the intermediate ocean. The study spans however a short time scale (40 years) given the slow response time and large memory of the ocean. Thus, instigating the investigation of ocean feedbacks in longer period experiments.

Hereof, our model based study is concerned in understanding the effects of sea ice reduction on the Arctic Ocean on a centennial time scale idealized simulations.

¹³ perturbations were introduced by reducing the sea ice strength parameter (P^*). Sea ice strength P is formulated as a function of ice concentration (A) and thickness (h).

1.6 Approach

Despite many observational efforts, the lack of understanding of the role and linkages between components of the Arctic climate system remains a challenge to be overcome. Model simulations may assist the investigation of these open questions, by solving a set of differential equations based on the basic laws of physics, fluid motion, and biogeochemistry. For this reason numerical modelling has become an essential component of climate research.

To address the impact of sea ice reduction on ocean circulation, isolated sensitivity experiments were carried out using a global coupled ocean-atmosphere-sea ice model (ECHAM6-FESOM). Ensembles consist of a set of simulations to which different physical perturbations were applied. It is important to emphasize that the sensitivity simulations are idealized experiments and should not be mistaken as predictions for future climate. Appropriate description follows in the upcoming section.

Chapter 2

Method

2.1 Model and Experimental Setup

The atmosphere ocean global coupled model (AOGCM) used to perform this study consists of the atmospheric and sea ice component ECHAM6 and the ocean Finite Element Sea-Ice Ocean Model component (FESOM). The coupling between the atmospheric and oceanic component is done by OASIS3-MCT. More information to this can be read in the work by [Sidorenko et al. \(2014\)](#).

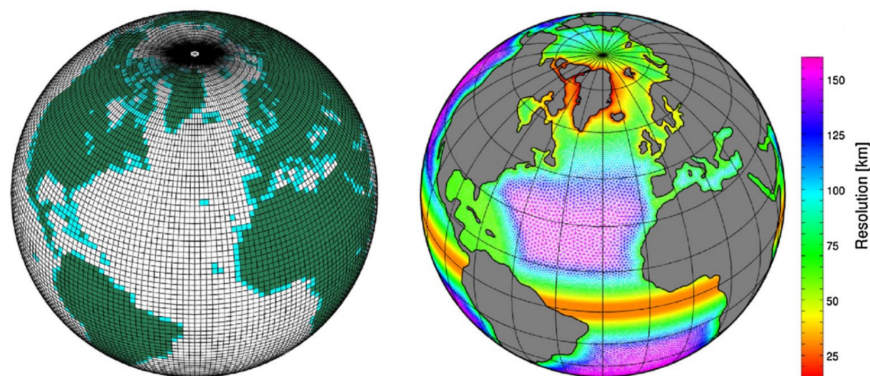


Figure 2.1: ECHAM6-FESOM mesh representation.

2.2 ECHAM

The atmospheric general circulation model ECHAM6 is the latest release of the ECHAM model developed at the Max-Planck-Institute for Meteorology in Hamburg. The implementation of ECHAM6 used in this work is run in a regular grid with 192 longitude, 96 latitude and T63¹, corresponding to an approximate $1.85^\circ \times 1.85^\circ$ horizontal resolution with 47 unevenly spaced vertical levels. It solves many parameters, from which twelve passed to FESOM (*i.e.* wind stress components (u,v) over ocean and ice, evaporation, shortwave radiation, sublimation, rainfall, snowfall, heat flux over ocean and ice, river runoff and calving). In addition, ECHAM6 solves the thermodynamics of sea ice. For more information see ECHAM6 documentation by (Stevens et al., 2013)

2.3 FESOM

FESOM has been developed at the Alfred Wegener Institute, Helmholtz Centre for Polar and Marine Research (AWI) over the last decade. It solves primitive dynamical equations of sea ice and ocean by addressing the momentum, continuity equations and geostrophic balance. It is based on unstructured-mesh methods, which confers the advantage refining the resolution in accordance to the research interest (Wang et al., 2014) (figure 2.2). In this study, the resolution ranges from 150 km, in open ocean region, to 25 km, in the Equator and coastlines (Figure 2.1). FESOM operates on 46 unevenly spaced z-levels in the vertical, which range from 10m in the upper 100m and gradually increase to 250m. More comprehensive description of the latest FESOM version is found in the works by (Wang et al., 2014). In the setup used, FESOM resolves the ocean and the dynamics of sea ice.

2.4 Sensitivity Simulations Setup

To assess the complex interaction and interdependency of the ocean-sea ice system a set of idealized experiments was carried out for a period of 150 years.

¹ The amount of truncations allowed in a wave representation of the variable. The translation of spectral space of T63 in regular grid point coordinate results in the aforementioned longitude and latitude numbers

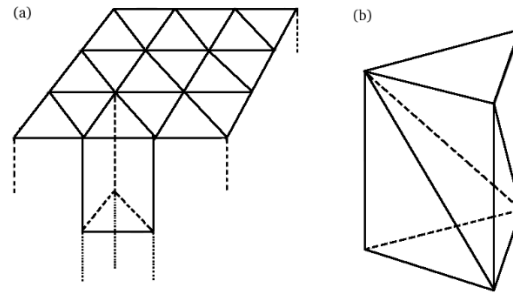


Figure 2.2: FESOM mesh representation: On a 2D plane the FESOM grid is represented by triangles, representing the face of a prism. On the 3D perspective the later forms tetrahedras in 3-D. Wang et al. (2014)

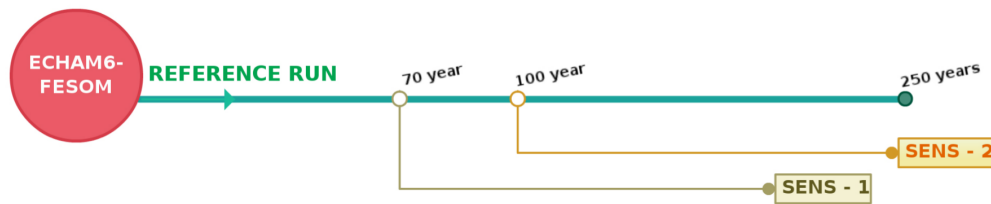


Figure 2.3: Scheme of simulation set up: A 250-year reference run (REF) run is branched off twice to create two sets of 150-year sensitivity experiments (SENS): SENS-1 initiating at year 70, and SENS-2 at year 100.

For the spin-up, the FESOM model was run for 60 years with atmospheric climatology from the second phase of Coordinated Ocean-Ice Reference Experiment (CORE II) for the year 1948 – 2007 based on the reanalysis from the National Center for Atmospheric Research (NCEP). Ocean initial temperature and salinity are derived from the World Ocean Atlas (WOA01). Subsequently, experiments were forced by values of greenhouse gases for the reference year of 1990.

After the ocean-only spin-up, the coupled model runs free and a 250 year reference simulation (REF) is produced. From this run three different physical perturbations are applied to the sea ice to create the sensitivity experiments (SENS). To evaluate the robustness of SENS results two sets of sensitivity runs are produced: SENS-1, after branching REF at year 70, and SENS-2 at year (Figure 2.3). In each SENS set, a different model parameter is perturbed with the aim of reproducing a moderate sea ice retraction (section 2.4). The response to each perturbation should however present a different seasonal dependence.

2.4.1 Added Longwave radiation experiment [LW]

The melt rate of sea ice is calculated from the net surface heat flux over ice and the conductive heat flux. Net sea ice surface heat flux (F_s) is described by the overall summation of four components: incoming and outgoing shortwave (SW) and longwave radiation (LW), and turbulent fluxes of sensible and latent heat (SH and LH , respectively) (equation 2.1). In the model, the downwelling SW and LW radiative fluxes are given by the atmospheric component of the model, whereas computed upward LW results from the Stefan-Boltzmann-Law, which describes the power radiated from a black body in terms of its temperature.

$$F_s = SW + LW + SH + LH \quad (2.1)$$

These experiments consist of the addition of 0.5 W/m^2 in the form of LW radiation exclusively to the surface of sea ice. This thermodynamical perturbation means a direct impact net surface heat flux (F_s) over the ice. Hence, it implicates an increased sea ice-atmosphere energy budget and triggers increased melting independent on any external forcing, and seasonal variations.

2.4.2 Reduced Albedo [ALB]

The albedo scheme for ECHAM6 includes important components such albedo decay due to snow aging (Stevens et al., 2013). Snow age and surface albedo have an inverse correspondence: while fresh snow has an albedo of 80 – 90%, old snow (melting snow) is much lower, on average 60%. Hence, increased snow ageing induces faster reduction of overall surface albedo (α). In this set of experiments, the snow ageing factor is multiplied by a factor of two. A reduced albedo represents more absorption of incoming SW energy (equation 2.2). This leads to increased melt and overall reduced sea ice thickness, concentration, and volume. Since perturbation is dependent on incoming solar radiation, a strong response during summer is expected.

$$SW \uparrow = \alpha \cdot SW \downarrow \quad (2.2)$$

2.4.3 Lead Closing Parameter [LEAD]

The *lead closing parameter* (h_0) is used in the parametrizations of the continuity equation for the sea ice concentration (S_A) (equation 2.3)² (Stevens et al., 2013). This parameter influences the relationship between vertical (h) and horizontal (A) sea ice growth. When solving sea ice formation, each grid cell of the model is covered by a maximum S_A that cannot exceed 100%. When h_0 is big, open ocean fraction term ($1 - A$) takes longer to close and, therefore, sea ice growth is mainly determined by the thickness rate of change term, and thicker ice is formed. On the contrary, if h_0 is small, the importance of horizontal growth overwhelms the vertical one, and open ocean fraction term ($1 - A$) leads the increase of S_A . Figure 2.4 illustrates the description above.

$$S_A = \frac{1 - A}{h_0} \cdot \left(\frac{\delta h}{\delta t} \right) \quad (2.3)$$

In our experiment, the parameter is reduced to half of its original range as shown in table 2.1. The reduction of leads (free interface ocean - atmosphere) creates a better insulation between ocean and atmosphere which dampens the heat exchange and causes a reduction in sea ice production. The consequence of this change is that open areas of sea ice close faster horizontally, rather than vertically. By the end of freezing season sea ice is thinner, thus is more vulnerable to melting as compared to thicker REF sea ice.

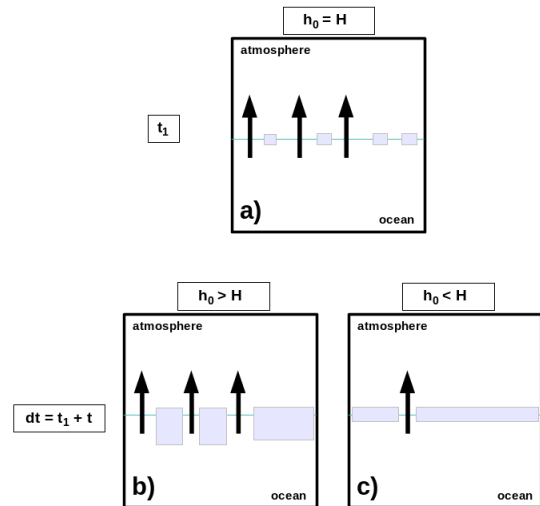


Figure 2.4: Scheme illustrating lead closing parameter perturbation. **a)** Sea ice at initial growth stage. **b)** Larger h_0 has more leads and sea ice grows thicker. **c)** Small h_0 reduces closes leads faster and sea ice is thinner.

² $\left(\frac{\delta h}{\delta t} \right)$ is the thickness rate of change, and $(1 - A)$ is the open ocean fraction

Table 2.1: Lead closing parameter range of values for reference (REF) and sensitivity (LEAD) runs

h_0	Minimum	Maximum
REF	0.5	1.5
LEAD	0.25	0.75

2.5 Output Evaluation

ECHAM6-FESOM outputs will be evaluated as follows: SENS simulations will be compared with REF, always accounting for corresponding period; that is, SENS-1 compares to REF years 70 to 220, and SENS-2 to REF years 100 to 250. The changes/differences are always calculated as SENS *minus* REF (SENS - REF).

The response of sea ice to each physical perturbation is assessed by analysing the changes of sea ice concentration (SIC), thickness (SIT), volume (SIV) and area (SIA). First, a time series analysis is conducted, and subsequently, the interpretation of sea ice difference maps is based on average values for late winter and summer.

To elucidate mechanisms influencing and responding to sea ice changes, atmospheric fluxes (from ECHAM6) and oceanographic properties and dynamics (FESOM) are evaluated. For such, spatial and temporal averaging intervals were defined. To have an insight on the trend of change three averaging periods were defined: from year 1 to 30 after SENS initialization, year 31 to 90, and year 91 to 150 (Ini30, Inter60 and Last60, respectively). Thirty and sixty year intervals are adopted to smooth the signal of annual to decadal variability. The averages of each period are compared to corresponding period in REF. For oceanic parameters three vertical levels were chosen: surface, upper layer average (50 – 230 m) and middepth average (230 – 1180 m). The analyses are based on difference maps.

Seasonal analyses were conducted initially, but no vigorous seasonally dependent differences between SENS runs were simulated. Therefore comparisons deal with the annual average response of the system.

In this work, the Barents Sea is defined as the area within 68 – 81°N and 17 – 67.5°E. This follows the definition by following [Årthun et al. \(2012\)³](#), however with a slight

³ 70 – 81°N and 15 – 60°E

zonal stretching to represent areas further east were reasonable reduction in sea ice cover is simulated in SENS experiments. Spatial air-sea fluxes averages are calculated presented in Chapter 3.

The comprehension of how changes in water properties and circulation in the interior of the Arctic Ocean affect the critical gateways to the Atlantic subarctic seas is done by the investigation of volume flux changes in sections 3.3.1 and 3.3.2.1. Volume flux is calculated as the spatial integral of the normal component of velocity across the section (v_n) (Equation 2.4).

Following, ocean heat budget results from the heat convergence of a closed mass budget will be presented in section 3.3.2.2. Thereby, four hydrographic sections enclosing the area of interest are defined. Heat flux is the product of (v_n), the difference of ocean temperature to a reference temperature (T_{ref}), the density of the water mass and the specific heat capacity of water (c_p) (Equation 2.5). To agree with recent studies, the reference temperature of 0°C is adopted.

$$V_{flux} = \int_s c_p \rho v_n ds \quad (2.4)$$

$$Q_{flux} = \int_s c_p \rho v_n (T - T_{ref}) ds \quad (2.5)$$

The results obtained in the second set of ensemble members, SENS-2 are shown in the initial discussion of sea ice results (section 3.1) and not are not discussed further. It is argued that the results agree qualitatively with those in SENS-1 experiments, and therefore confirm the robustness of the simulated responses. Trivial differences outcome from the commitment of changes to natural variability: larger differences are seen in the second averaging period (Interm60), which overlaps the third (Last60) of SENS-1. In spite of that, distribution of patterns and magnitudes allow a direct comparison with SENS-1 and thus confirm the reliability of the results. Tables, difference maps and plots are included in the Appendix B.

Statistical significance of the sensitivity experiment will be assessed for all maps and section which show difference between the two experiments (*i.e.* SENS - REF). To test if the mean of the difference between the runs is different from zero, *Wilcoxon Signed Rank* test for paired differences of dependent samples (Wilcoxon, 1946) was employed. If the p-value is small, the hypothesis that the difference is due to chance can be rejected, and thus, it can be concluded that the sensitivity has a median distinct from the reference run. Year-to-year differences have been calculated respective to each averaging period, and all discussed differences lay within the 98% confidence level.

Chapter 3

Results and Discussion

This chapter begins with presenting and discussing sea ice results (section 3.1). Given that any changes in the sea ice cover will necessarily impact the ocean-air interaction, an evaluation of air-sea fluxes is conducted (section 3.2). Finally, new results on the impact of sea ice retraction on the Arctic oceanic circulation are presented (section 3.3.1), with focus on the relative role of Atlantic gateways on volume and heat exchanges (section 3.3.2).

To demonstrate how REF model simulation compares with relevant observations, the initial years of simulation are compared with observations as indicated. Accordingly, the discussion of ocean heat and volume flux changes is supported by comparison with observations and model based studies. These comparisons are conducted with the aim of understanding the representation of the system by our model configuration, and putting results into perspective. Nevertheless, it should be kept in mind that this is an isolated sensitivity study and comparisons with observations and predictive studies are done to put results into perspective.

3.1 Sea ice

Observations and model

Prior to any SENS experiments result analysis, REF outputs are compared with passive microwave remote sensed sea ice area (SIA) data, and sea ice volume (SIV) from a

model simulation carried out with data assimilation, as described next.

SIA is calculated as the sum over all ocean grid elements of the product of ice concentration and grid element area. Sea ice concentration (SIC) time series were retrieved from a combination of observations from the Special Sensor Microwave/Imagers (SSM/Is) flown on a series of Defense Meteorological Satellite Program missions (Cavalieri and Parkinson, 2012).

The estimation of SIV from observational data sets is hindered by the lack of large spatial and temporal coverage of the sea ice thickness (SIT). Therefore, the estimation of the model performance in hereby done using the SIV time series provided by the Pan-Arctic-Ocean Modelling and Assimilation System (PIOMAS)¹ (Zhang and Rothrock, 2003).

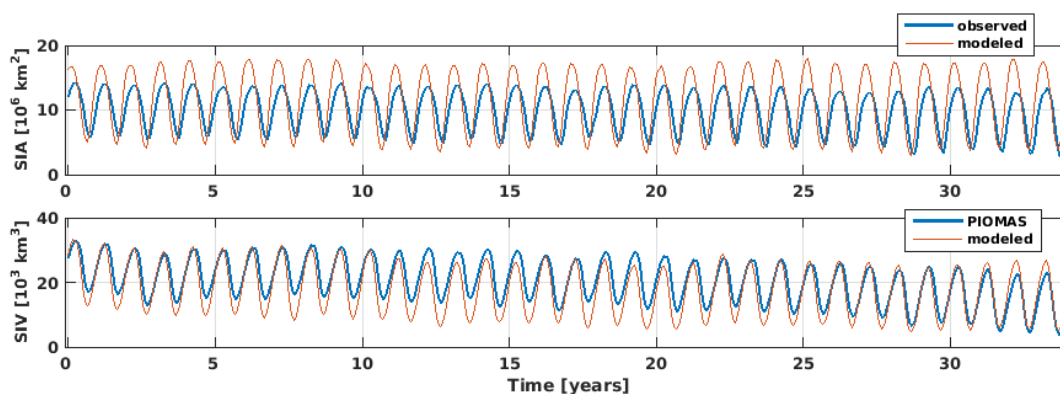


Figure 3.1: First 34 years of REF simulation against **a)** SIA from satellite measurement (observed – NASA) and **b)** SIV from assimilated model data (PIOMAS).

A qualitative evaluation reveals that REF set up has a much more pronounced annual cycle, with overestimated winter SIA and underestimated summer SIV (Figure 3.1), when compared to 1979 to 2013 observational data.

To have a better understanding of simulated features, 30-year averaged March (maximum) and September (minimum) maps of sea ice concentration (SIC) is shown in Figure 3.2. Sea ice extent climatology provided by the NSIDC (Figure 3.3) allow qualitative comparisons. REF run SIT average maps for the same period have been compared against Cryosat observations (not shown).

¹ A sea ice-ocean coupled model with assimilated SIC observations and SST in the ice free regions.

The main characteristics of sea ice are well reproduced: thicker multi-year sea ice and higher summer SIC occur on the western basins, while further away from the Canadian coast sea ice cover reduces in thickness and concentration. Similar to the observations, the marginal areas have seasonal coverage. Some regional winter over-estimation of sea ice is seen in the southern Barents sea. This bias is not a exclusive feature of ECHAM6-FESOM; [Smedsrud et al. \(2013\)](#) draws attention to the fact that more than half of global models show similar results.

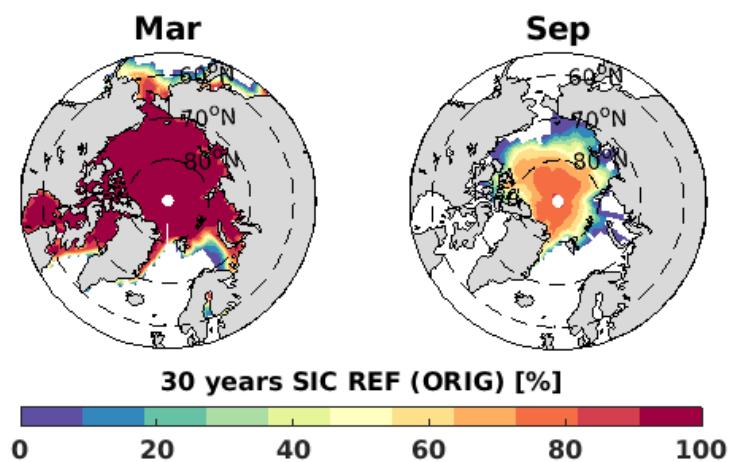


Figure 3.2: REF run average 30-year SIC for months of maximum and minimum sea ice cover. **ORIG** indicating avergaing period from year 70 to year 100 after experiment initialization.

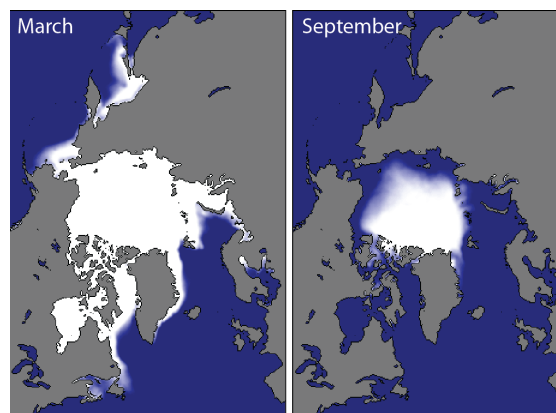


Figure 3.3: Climatological maximum (Mar) and minimum (September) sea ice extent from NSIDC for the years 1981 – 2010

Comparative analyses:

Sensitivity runs (SENS) and Reference run (REF)

In all SENS experiments a sea ice reduction is simulated. The time series of Arctic averaged SIA and SIV are shown in Figures 3.4 and 3.5 to evaluate how SENS simulations depart from REF. To reduce the amplitude of high frequency variability a 5-year moving average filter was applied.

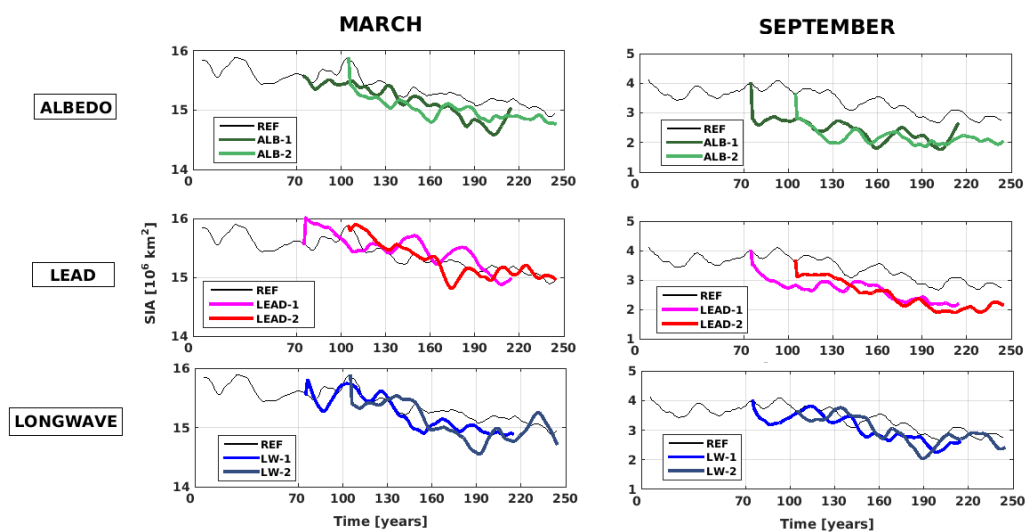


Figure 3.4: Sea ice area time series. Subplot of 5-year running mean reference run (REF) against pairs of ensemble members (from top to bottom: ALB, LEAD, LW).

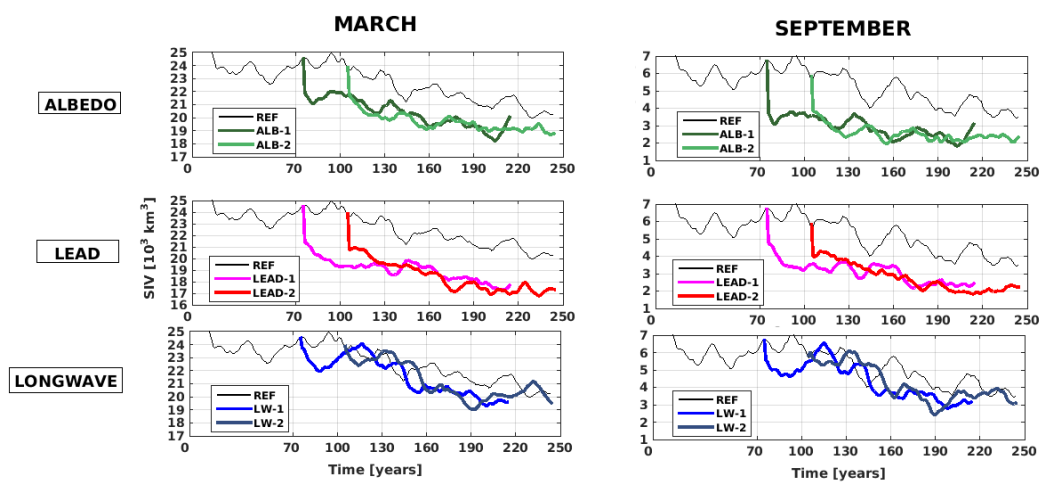


Figure 3.5: Sea ice volume time series. Subplot of reference run (REF) against pairs of ensemble members (from top to bottom: ALB, LEAD, LW).

A decline trend of sea ice is identified not only in the perturbed runs, but also in REF. This indicates that an equilibrium state for the 1990 greenhouse forcing is not reached during the 250 years of simulation, suggesting the slow response time of the climate system. Nevertheless, this does not invalidate our findings since all analyses are performed on a comparative basis.

A swift change of sea ice state occurs within the first years of SENS simulations after branching off from REF. The response appears qualitatively very similar in all six SENS experiments. Subsequently, the new state of ice develops in parallel to that in REF. Table 3.1 indicates this result as the percentage change of mean SIV between SENS-1 and REF in Ini30, Interm60 and Last60.

Reduced albedo (ALB-1, ALB-2) experiments present a clear summer (September) change with pronounced SIA and SIV retraction. Although lesser changes of SIA occur in winter (March), overall loss of thickness drives a significant retraction of winter SIV. Accordingly, LEAD-1 and LEAD-2 simulations undergo summer SIA and SIV reduction. The seasonal dependence of the perturbation is imprinted in the subtle increase of SIA seen in winter (March). This, however, does not compensate the thinning of ice, and SIV is reduced the most by this set up. LW-1 and LW-2, in contrast, do not create very large differences in comparison to REF neither in SIA nor in SIV, and as expected no seasonal dependent signal is evident. Table 3.1 gives the relative SIV reduction² of each SENS experiment referenced to the average absolute values of the REF simulation.

Figure 3.6 shows the development within Ini30 period of SIA and SIV as climatological monthly means, with error bars associated with year-to-year standard deviation. It is important to recall that the REF run is also undergoing a sea ice reduction trend, thus committing the analyses of annual variability. In REF simulation SIA undergoes much less year-to-year variation, whereas SIV averages oscillates more heavily. Therefore the thickness is the most sensitive property of the ice in our simulations.

The pronounced SIA annual cycle in REF is hardly changed in SENS experiments. SIV experiences retraction throughout the year in all SENS simulations. LEAD shows the largest SIV decline from December until May. Once summer sets in ALB suffers the strongest declines and reaches the same state as LEAD from June to November. LW

² $\left(\frac{\text{SENS} - \text{REF}}{\text{REF}} \right) \cdot 100$

changes are less important, with associated error bars somewhat overlapping those in REF. The error bars indicate that the standard deviations in Ini30 are larger in REF, suggesting year-to-year variability is damped by physical perturbation introduced in SENS.

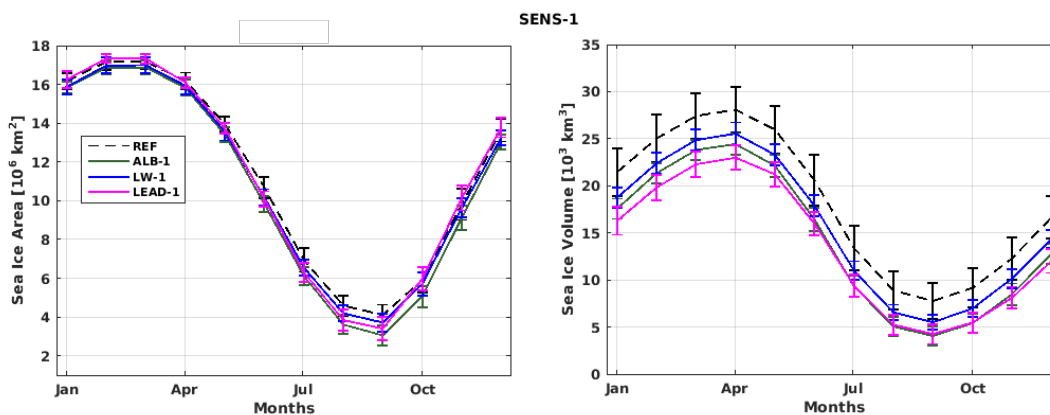


Figure 3.6: SENS-1 development within Ini30 of SIA and SIV as climatological monthly means, with error bars associated with year-to-year standard deviation

Table 3.1: Sea ice Volume: REF: Annually averaged absolute values [10^3 km^3] and SENS: annually averaged relative change³

Year	1 – 30y	31 – 90y	91 – 150y
REF	17.42	15.85	14.54
LW-1	10.4%	2.5%	10.6%
ALB-1	18.3%	16.1%	16.4%
LEAD-1	22.0%	20.6%	21.6%

The evaluation of 150-year average difference maps for SIT and SIC show that the three SENS experiments qualitatively simulate very similar sea ice change patterns on seasonal average (Figure 3.7, Figure 3.8). A consistent reduction of SIT over values in REF (Figure 3.7a) throughout the year is a common outcome of all SENS experiments (Figure 3.7b,c,d). Winter decrease is the largest in LEAD and does not exceed 0.5 m, and summer local differences in the Canadian Basin are up to 1 m in LEAD and ALB. LW perturbation is the less impacting, and produces qualitatively similar SIT reduction on summer and winter with values not greater than 0.15 m.

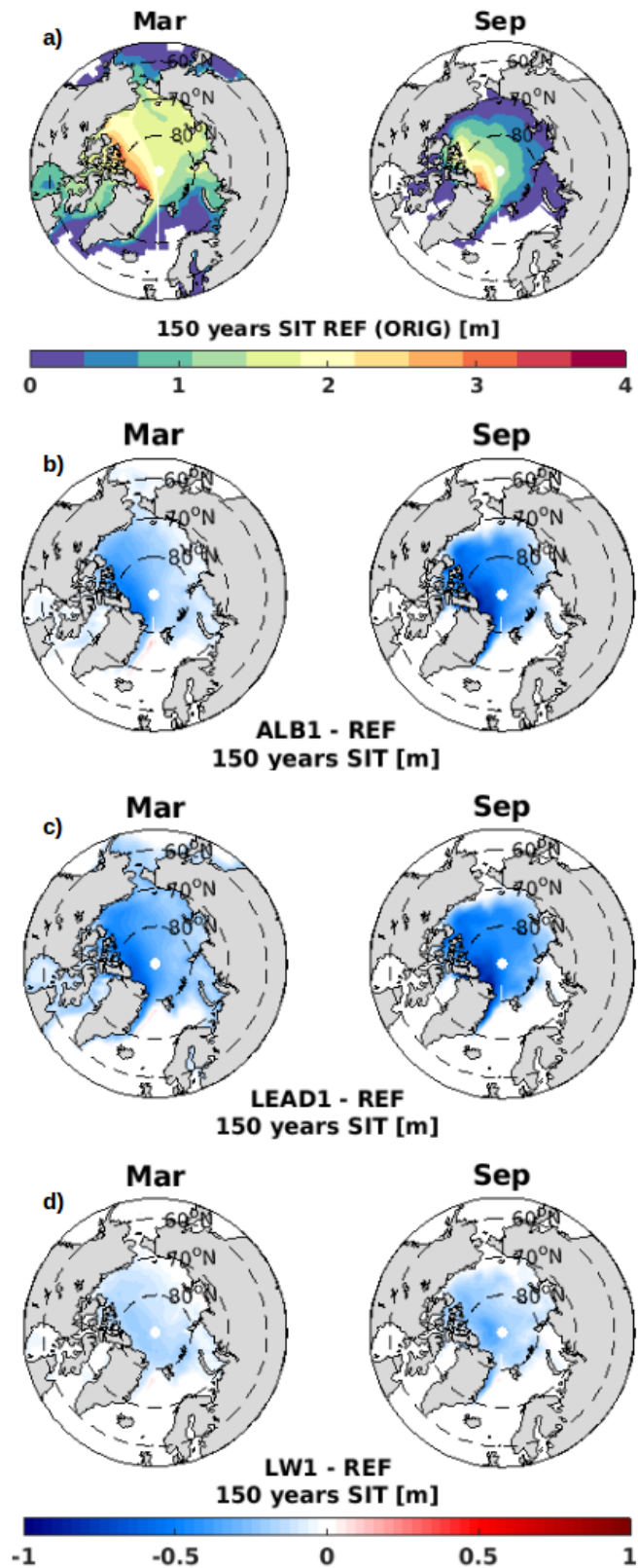


Figure 3.7: Sea ice thickness (SIT): 150 year absolute values (REF) and difference maps (SENS-1 - REF). (ORIG) indicating averaging period from year 70 to year 220 after experiment initialization.

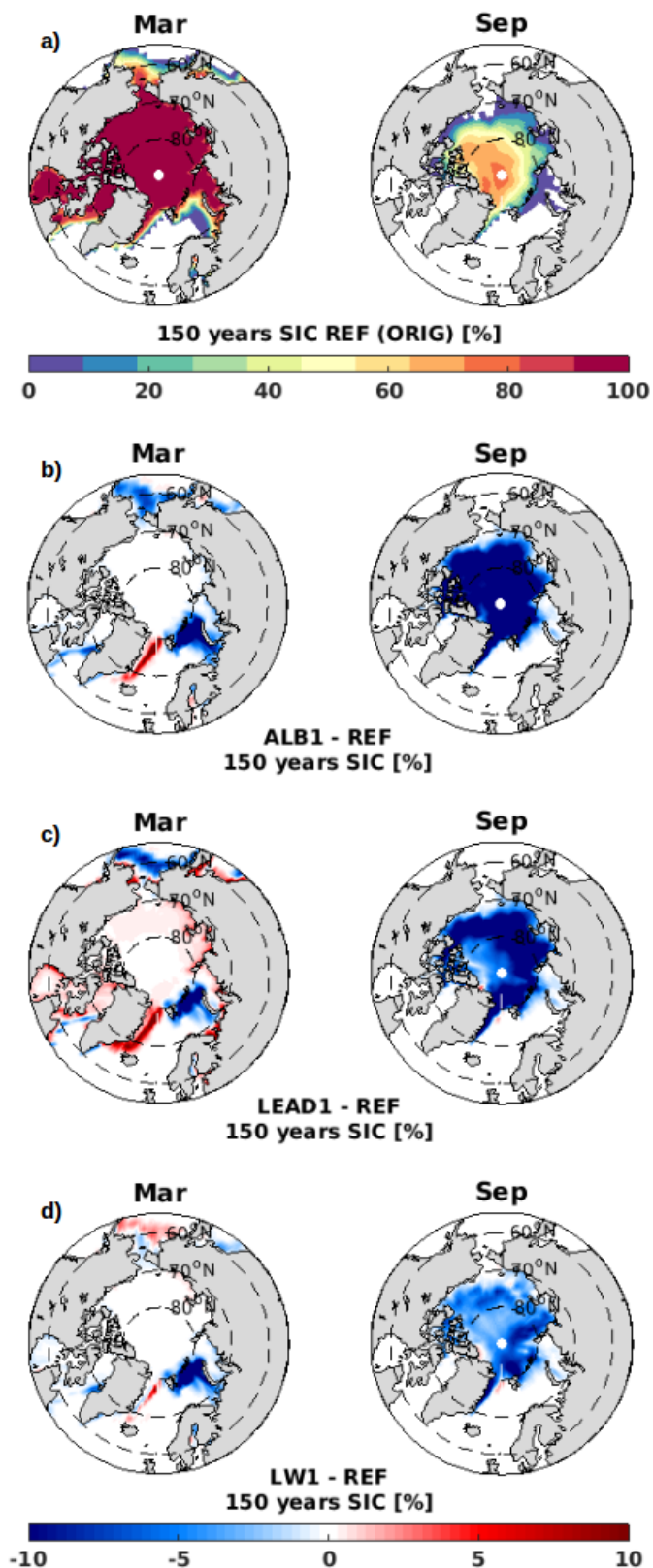


Figure 3.8: Sea ice concentration (SIC): 150 year absolute average (REF) and difference maps (SENS-1 - REF). (ORIG) indicating averaging period from year 70 to year 220 after experiment initialization.

SIC difference between SENS simulations is fundamentally explained by each physical perturbation introduced (in detail in section 2.4). While in ALB the strongest difference over REF is established for the summer SIC decrease (Figure 3.8b), in LEAD a strong winter (March) increase in SIC is simulated (Figure 3.8c). In turn, the LW simulation creates neither a seasonal dependent nor strong difference (Figure 3.8d). All in all, SIC are somewhat comparable in terms of patterns between each SENS experiment, and annual average differences between SENS and REF show that loss of SIC overwhelms any seasonal increase within the Arctic.

During winter the Arctic Ocean sea ice reduction largely reflects variations in the Barents Sea ice cover, where a strong (up to more than 20%) decrease in the northern area is simulated in all SENS experiments. This result agrees with recent observations (Serreze and Barry, 2011; Vihma, 2014).

Increased SIC over Eastern Greenland slope is most likely an outcome of a dynamical feedback rather than caused by local intensification of sea ice formation. Thinner sea ice produced by the thermodynamical perturbations in SENS breaks up and crumbles more easily under the same wind stress and ocean currents, and therefore, it becomes more mobile.

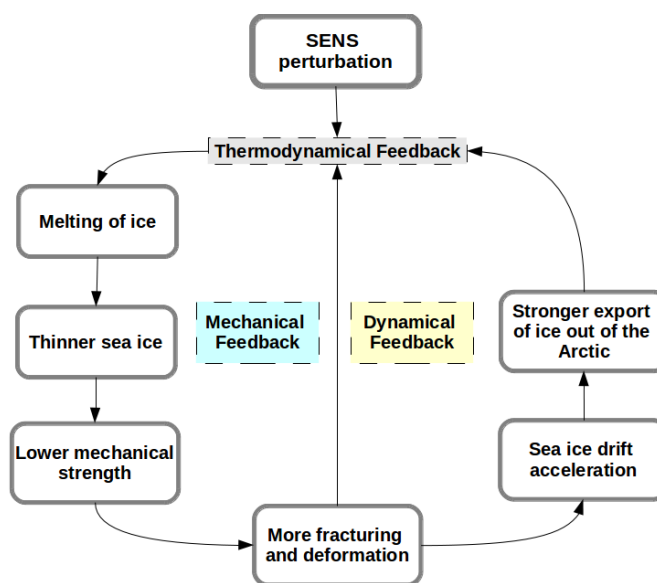


Figure 3.9: Feedback loops: thermodynamical feedbacks are dependent on perturbation, but all lead to thinning of all and for this reason, mechanical and dynamical feedback are comparable in all simulations.

Also, thinner and fractured sea ice permits increased momentum exchange between atmosphere and ocean. In this work it is proposed that the reduction of sea ice is the crucial trigger for a sequence of ocean circulation changes across Fram Strait and in the Barents Sea. (Figure 3.9).

3.2 Atmosphere

Atmospheric Circulation

Even though it has been shown by [Deser et al. \(2015\)](#) that atmospheric circulation of the northern hemisphere is highly sensitive to sea ice distribution and sea surface temperature (SST) in the subarctic ocean, no change of circulation patterns was observed in the sensitivity simulations performed for this study, when compared to REF.

Difference maps of wind speed and mean sea level pressure suggest no consistent response between SENS experiments, despite the computation of some statistically significant differences (not shown). There is too much variability in the atmosphere and reactions to the perturbations are too small.

Air-Sea Fluxes

The anomalous loss of sea ice opens the ocean to stronger atmospheric forcing, and accelerates ongoing feedback mechanisms. Areas experiencing large sea ice reduction are coupled with air-sea-ice system warming. In this work, nearly the entire Arctic region experiences air temperature warming near the surface (2-m temperature, TSURF) with exception of the area undergoing SIC increase over eastern Greenland. Most pronounced changes are concentrated over the Barents Sea and the GIN Seas, where differences are significant at a 98% confidence level.

Accordingly, differences in net heat flux⁴ between ocean and atmosphere are more pronounced over the aforementioned areas. The reduction of sea ice cover in northern part of Barents Sea, simulated in all SENS experiments, facilitates an increased mean absorption of SW by the ocean in late spring and late summer (from April to June

⁴ NET = SW + LW + SH + LH

and from July to September) when compared to REF (not shown). As a consequence, seasonal late autumn (October to December) and winter (January to March) LW loss is larger in SENS simulations. Winter warming contributes strongest to the annual average TSURF increase over the Barents Sea. Averaged over the three sensitivity experiments (SENS-1) the Last60 difference amounts to $+0.7^{\circ}\text{C}$ in August and $+1.9^{\circ}\text{C}$ in February. This result corresponds to nearly half of the 21st century projections of a summer warming up to 3.7°C over the Barents Sea [IPCC \(2007\)](#). This suggests that changes in sea ice conditions play a big role in local warming and amplification. In a recent work by [Koenigk and Brodeau \(2013\)](#), the projection of TSURF changes are strongly related to modification in sea ice state and heat fluxes. From CMIP5⁵ future simulations with EC-Earth model, the later study obtains local annually averaged warming in the Barents Sea region between 10 and to 17 K⁶, depending on the greenhouse gases emission scenario⁷.

Nevertheless, the radiative terms (namely, SW and LW) roughly balance out each other over the Barents Sea, and the net annual heat flux changes from Ini30 to Last60 are consequence of turbulent heat flux (SH and LH) adjustment. Values in [Table 3.2](#) represent the spatial average corresponding to the Barents Sea area. LH and SH fluxes from the ocean to the atmosphere are increased in all SENS when compared to REF. This is due to the combined effect of sea ice cover reduction and ocean warming. Ocean properties are discussed in the upcoming section.

The balance between precipitation and evaporation (P-E) is essentially positive over the Arctic domain in REF. In all SENS simulations, distribution of P-E changes looks rather patchy. Even so, some consistent changes between SENS and REF are seen in the Last60 period, and changes significant at a 98% confidence level are restricted to areas of larger changes of sea ice cover and in the GIN Seas. Evaporation increase overwhelms precipitation changes and over the Barents Sea, and Last60 anomalies reach up to 0.6 mm/day, over average REF values of 0 – 1 mm/day.

⁵ Coupled Model Intercomparison Project Phase 5

⁶ Considering this values are describe with a comparative character, one can also state: 10 – 17 °C

⁷ Representative Concentration Pathways (RCP) 2.6, 4.5 and 8.5 emission scenarios. The RCPs are named according to the radiative forcing target level at year 2100. More information in [IPCC \(2013\)](#).

Table 3.2: Net spatial average Turbulent Heat Flux over Barents Sea

Avg.Period	[TW]	BS			
		REF	ALB-1	LEAD-1	LW-1
1 - 30	TH ↑	113	113	114	115
	NET ↓	74	72	75	76
31 - 90	TH ↑	120	129	127	127
	NET ↓	81	89	86	86
91 - 150	TH ↑	132	145	146	142
	NET ↓	92	105	106	103

TH: Turbulent Heat = SH + LH
NET: SW + LW + SH + LH
↑ : from ocean to atmosphere
↓ : from atmosphere to ocean

3.3 Arctic Ocean Circulation

After discussing how sea ice and air-sea fluxes are reacting to perturbations in each SENS experiment, this section conducts the evaluation of the ocean hydrography and dynamics outcome. First, a condensed overview of temperature and salinity changes is presented and discussed, followed by the survey of outcomes in the main Arctic - Atlantic gateways.

3.3.1 Hydrography

Surface Ocean

The values of sea surface temperature (SST) and sea surface salinity (SSS) in REF experiment resemble reasonably well observational data, and agree with overall characteristics given in section 1.2.

The surface layer in the interior of the Arctic Ocean simulated in REF has SST values lower than 2°C and SSS less than 32 psu. In turn, the AW reaching the GIN Seas is warmer than 3°C and saltier than 35 psu. These values resemble reasonably well the upper layer of the vertical structure in Figure 1.2.

Difference maps (SENS - REF) of SST Figure 3.10 suggest no change in the interior of the Arctic Ocean is induced due to the increased sea ice melt. However, a smooth to substantial warming prevails over shelf and subarctic seas.

In the Atlantic subarctic sector, on the other hand, SST increase up to 2°C. The prior analysis (section 3.2) of local radiative balance changes suggest this anomaly is mostly driven by modification of water properties upstream. This argument is supported by the fact that in SENS simulations the North Atlantic subpolar gyre is shifted somewhat southeastward, and consequently displaces the pathway of surface and subsurface waters flowing northward. Changing NAC route affects the amount of sensible heat exchange taking place between ocean and atmosphere: if the current is displaced southward the thermal gradient between the ocean and the air is reduced, thus less energy will be given off by the ocean water and, thus the waters within NAC and later the NwAC have higher temperature in SENS than in REF (shown in Appendix B, Figure B.7).

The largest changes in SSS (Figure 3.11) are fundamentally different to those of SST, and besides, are already seen in the Ini30 period. Meltwater from thick multi-year ice is usually advected to the Beaufort Sea (Carmack et al., 2015). The build up and accumulation of freshwater anomaly in the interior of Beaufort Gyre is a consequence of the enhanced Ekman convergence of the anticyclonic circulation and results in a positive sea surface height (SSH) anomaly (Figure 3.12).

A SSS increase is observed in shallower basins, where mainly over Kara, Laptev and East Siberian seas strong positive salinity differences are translated into robust decrease in SSH. The substantial increase over shelf seas and MIZ can be a consequence of local sea ice growth rate change. Another possible reason for the large SSS differences is simply the response to the increased trapping of freshwater inside the gyre due to the enhanced circulation, along with the increased Transpolar Drift which pushes water from the Kara, Laptev and East Siberian Sea. Thereafter, the changes in SSS could be a simple response to the dynamical change of the ocean rather to thermodynamics of sea ice. Over GIN seas and Barents Sea the increase in salinity can be a response to local enhanced evaporation. Salinity changes are not further investigated in this work.

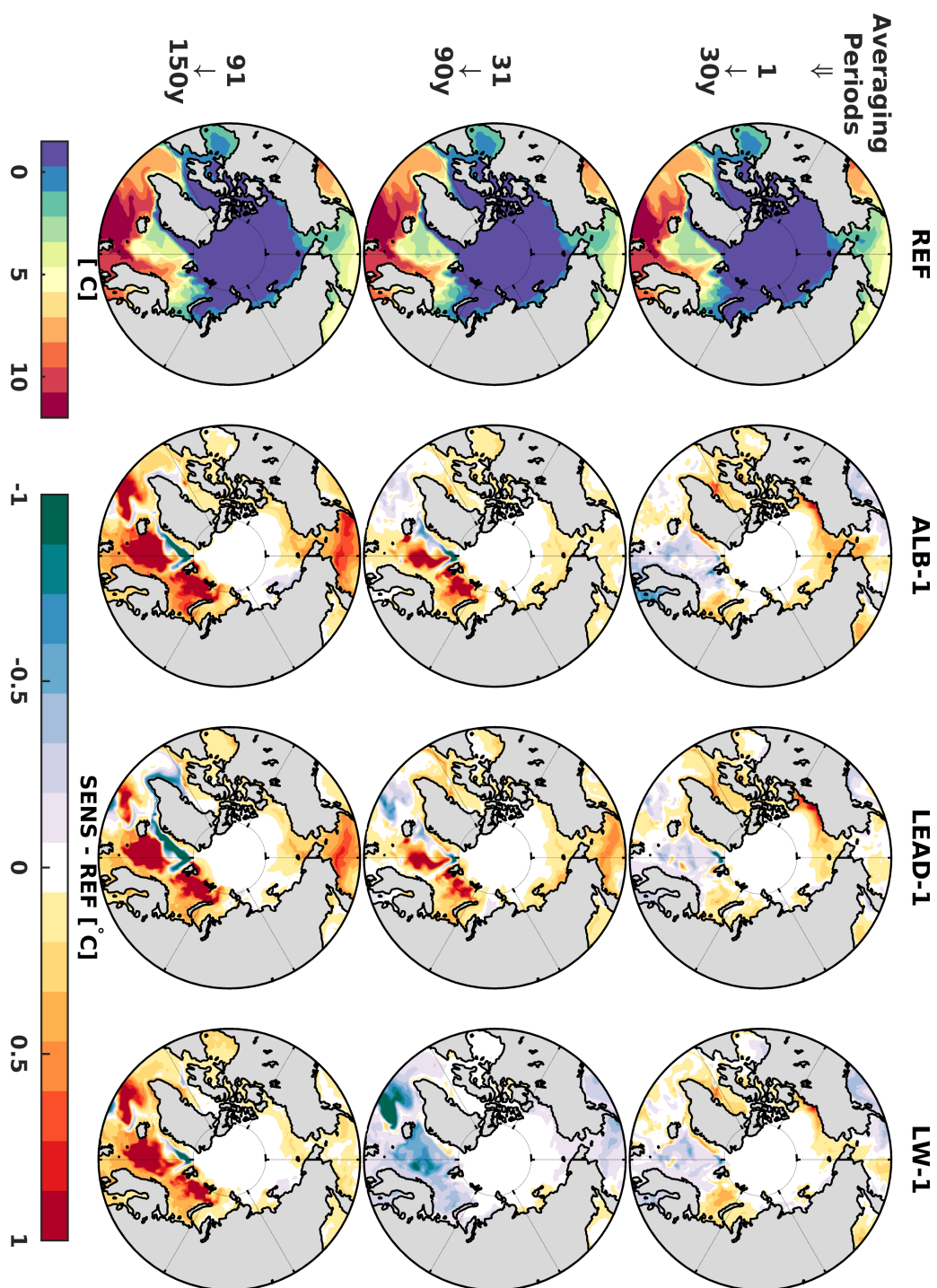


Figure 3.10: Average SST north of 55° N. From top to bottom: Ini30 (1 – 30y), Interm60 (31 – 90y) and Last60 (91 – 150y). Column I: Absolute values for REF run. Columns II - IV: difference maps between SENS-1 and REF as indicated.

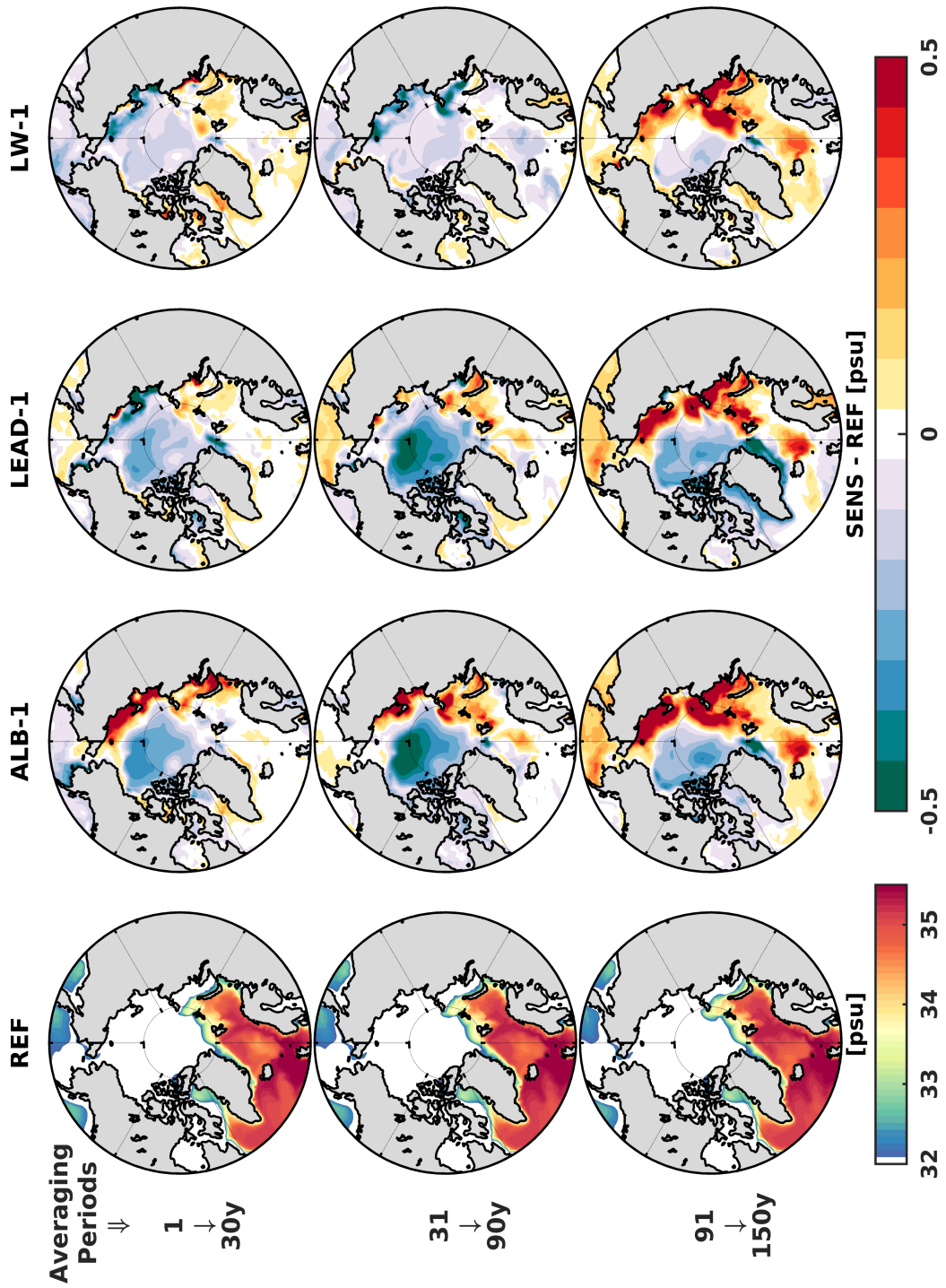


Figure 3.11: Average SSS north of 55° N. From top to bottom: Ini30 (1 – 30y), Interm60 (31 – 90y) and Last60 (91 – 150y). Column I: Absolute values for REF run. Columns II – IV: difference maps between SENS-1 and REF as indicated

SSH results from the integration of the density field over the entire water columns, and anomalies can be interpreted as proxies for changes in the mean geostrophic flow changes. In Figure 3.12, the patterns of SSH changes in the center of the Arctic Ocean indicate clearly the spin-up of the anticyclonic Beaufort Gyre, and the strengthening of the Transpolar Drift. The combined effect of increased sea ice mobility with enhanced circulation explains the increased SIC in the eastern Greenland slope, and suggests an increased outflow of melt water/ freshwater through the Fram Strait.

The changing trend differs essentially for the LW-1 experiment, in which a pronounced cooling anticipates the warming in the last 60 years of simulation. Still, differences between SENS and REF are very similar in all experiments in Last60. This strongly suggests the ocean as the controlling agent in damping and reacting to the different perturbation.

Average differences of ocean temperature and salinity between 50 and 230 m are not discussed, since they merely differ quantitatively from the surface changes.

Middepth Ocean

In accordance to [Itkin et al. \(2014\)](#), middepth (here 230 – 1180, in the referred work 212 – 1200m) average differences of the initial decades (in this work, 30 years, in [Itkin et al. \(2014\)](#) 40 years) simulate a strong cooling signal within the Arctic Ocean in the idealized sensitivity experiments. In the present work, negative anomalies are restricted to the westernmost part of the Eurasian Basin, against a spread cooling throughout the central basin in the aforementioned work. The temperature response within the interior of the Arctic Ocean/Beaufort Gyre and Canadian Basin begins to appear forward in time, and is more pronounced in the last 60 years average. At this stage our results differ substantially from those in [Itkin et al. \(2014\)](#), thus suggesting the relevance of long timescale simulations to the coupled response and adjustment processes of the system.

3.3.2 Volume and Heat fluxes

After identifying and presenting some evidences of circulation changes triggered by sea ice loss, a closer investigation of how these changes propagate towards the North

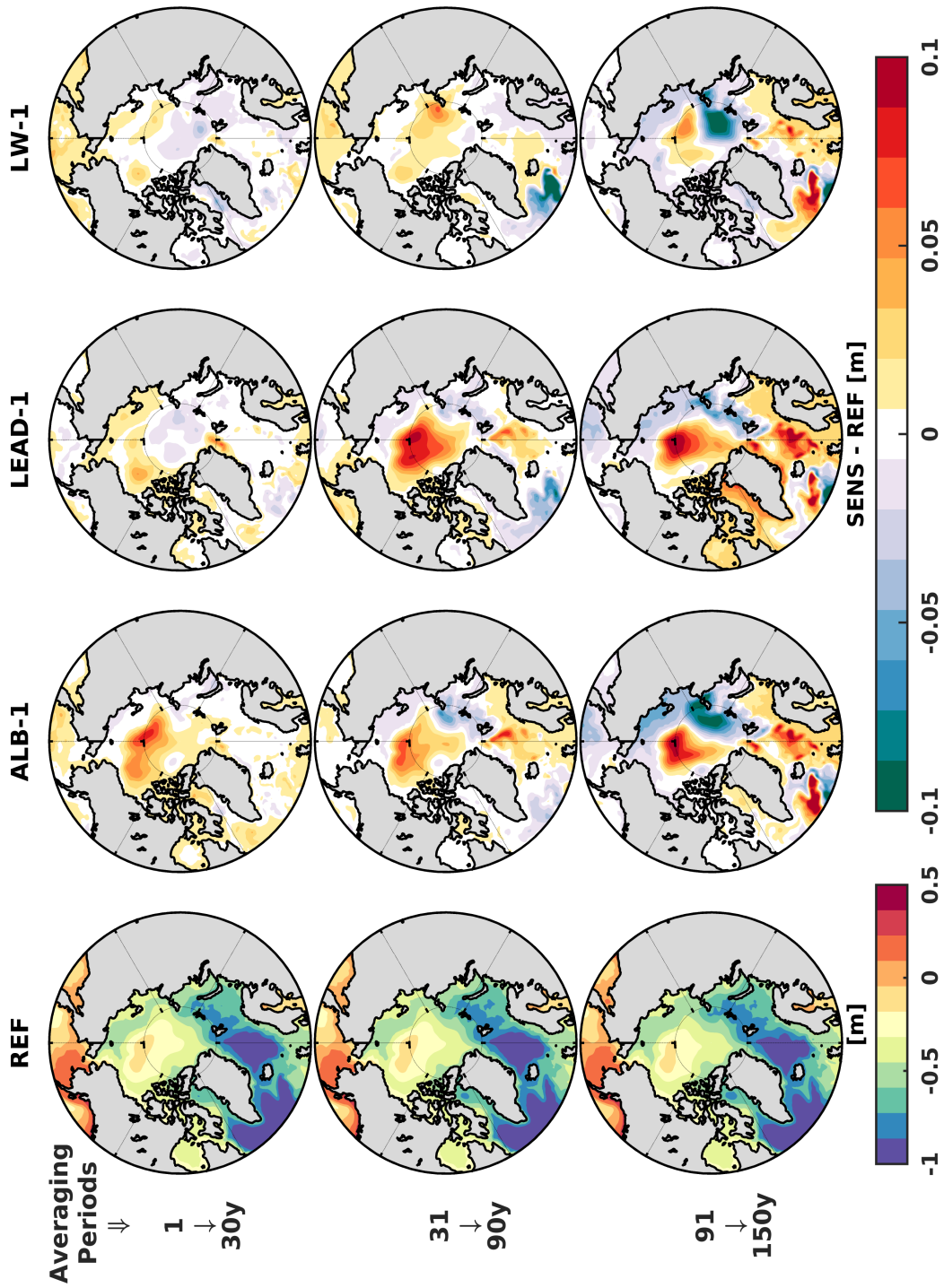


Figure 3.12: Average SSH north of 55° N. From top to bottom: Ini30 (1 – 30y), Interm60 (31 – 90y) and Last60 (91 – 150y). Column I: Absolute values for REF run. Columns II – IV: difference maps between SENS-1 and REF as indicated

Atlantic is done here. The associated changes in volume flux across the two critical Atlantic gateways were quantified. Anomalies of comparable sizes but opposite signs were computed; that is, increase inflow into the Barents Sea and outflow through FS. Simple correlation were computed and values were the largest for instantaneous response (not shown).

3.3.2.1 Fram Strait: Volume Transport out of the Arctic

The velocity of the EGC flowing southward is fairly stable in REF from Ini30 to Last60 period, and has a speed of ca. 10 cm/s. Difference velocity across the section at 78.5° N plots indicate the increase of outflow from the Arctic Ocean, and so, support the outcome of enhanced circulation suggested by SSH gradients mentioned in section 3.3.1. (Figure 3.13)

The upper 500m of the water column speeds up in all SENS experiments already in Ini30 period. From Ini30 to Last60, southward velocities cover a larger vertical and horizontal area of the layer, with the largest anomalies reaching up to 5 cm/s. Likewise, an increasing northward trend in the east of the section is also simulated. The AW inflow (WSC) is confined more to the eastern portion of the strait and, in turn, speeds up. While differences agree qualitatively between all SENS and REF, LEAD experiments drive the largest changes, followed by ALB and, lastly, LW.

Along with increased southward speeds, a substantial cooling and freshening (Figure 3.14) of the upper layer outflow occurs in all SENS. Upper water with temperature between -1°C and 0°C and salinity up to 33 psu in REF simulation, cools to temperatures of Arctic Surface Waters (*i.e.* $< -1.5^{\circ}\text{C}$) and, accordingly, average salinities are reduced by up to 0.8 in Last60 in all SENS experiments. In contrast, the AW is warmer and with higher salt content. These differences however do not exceed 0.5°C and 0.1 (when comparing Last60 averages).

Velocity differences in the lower layer (from 500 m to the bottom) indicate slowdown of the recirculation branch of AW. This result suggests that the increased exchange of water occurring in the upper layer is counterbalanced further below. Mechanisms behind the changes need to be assessed for solid understanding, and are not discussed in this work.

Salinity increase and warming of the waters below 500 m are comparable between all SENS experiments. The increasing trend simulated is consistent with an advective signal of the changes upstream as discussed in section 3.3.1. Ini30 and Interm60 differences show positive anomalies concentrated on the eastern side of the strait. This signal spreads zonally in Last60, suggesting the anomalies advected within the AWL are mostly exported from the Arctic Basin over the last simulation decades.

Average REF net volume flux at a 78.5° N section across Fram Strait compare relatively well to recent observational estimates of 2 Sv to the south (Schauer et al., 2008). The analysis of changes of inflow and outflow, is particularly critical in our study. Due to the fact that water column from 500 to bottom has inflow and outflow velocities reducing in all SENS, a negative trend of integrated flux in both directions is calculated. However, an analysis of the upper layer changes suggest the opposite. Differences of the net volume flux through the Fram Strait section are indicated in Table 3.3. (Table C.1 depicts contribution of changes of the integrated inflow and outflow to the net volume flux.)

Table 3.3: Averaged net Volume Flux changes through Fram Strait section. REF: absolute values are positive directed to the south. SENS values denote difference between averages (SENS - REF).

Year	1 – 30y	31 – 90y	91 – 150y
REF	2.32 ± 0.80	2.43 ± 0.84	2.88 ± 0.88
ALB-1	−0.01	0.42	0.78
LW-1	−0.07	0.25	0.44
LEAD-1	0.04	0.34	1.08

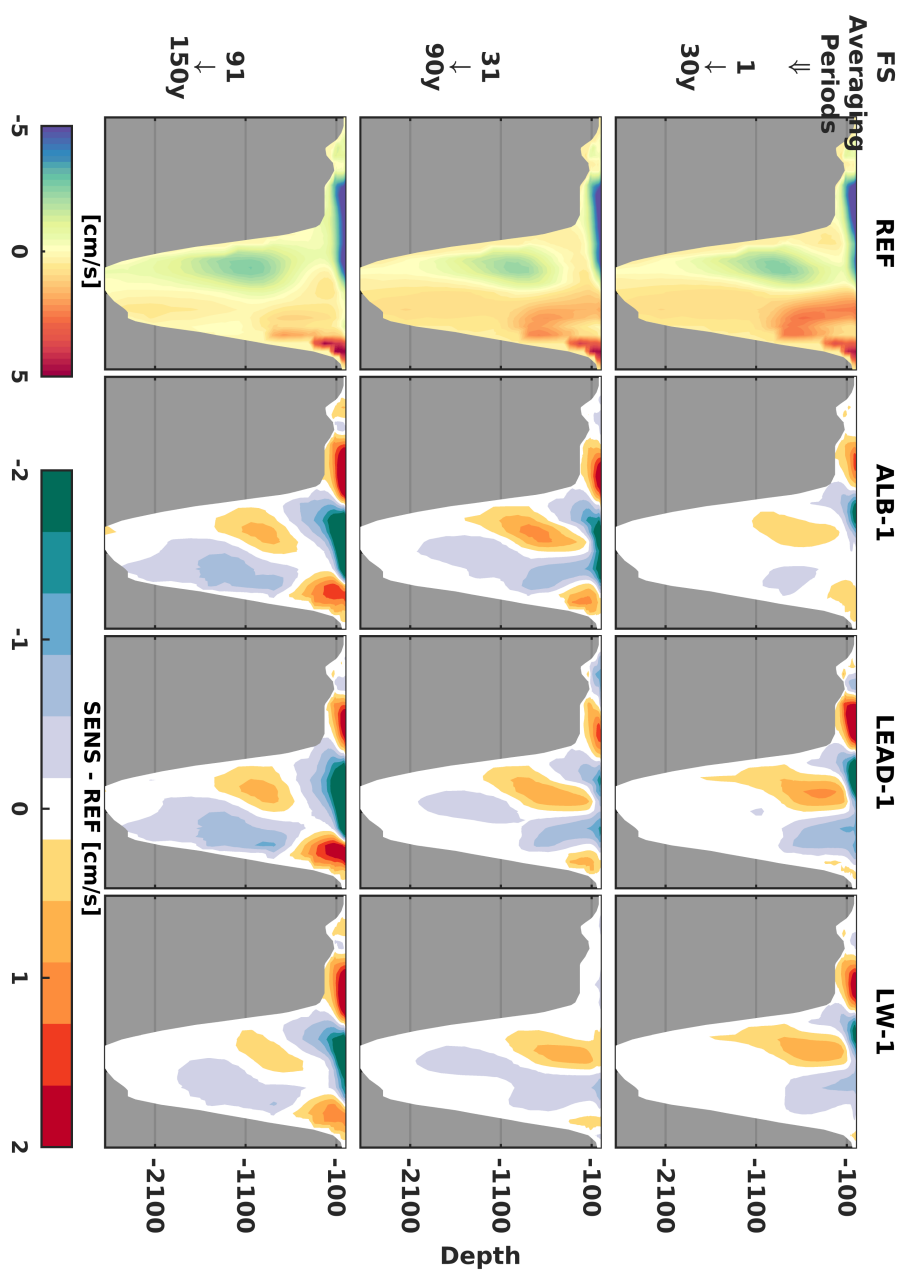


Figure 3.13: Velocity across Fram Strait section. From top to bottom: Ini30 (1 – 30y), Interm60 (31 – 90y) and Last60 (91 – 150y). Column I: Absolute values for REF run. Columns II - IV: difference maps between SENS-1 and REF as indicated.

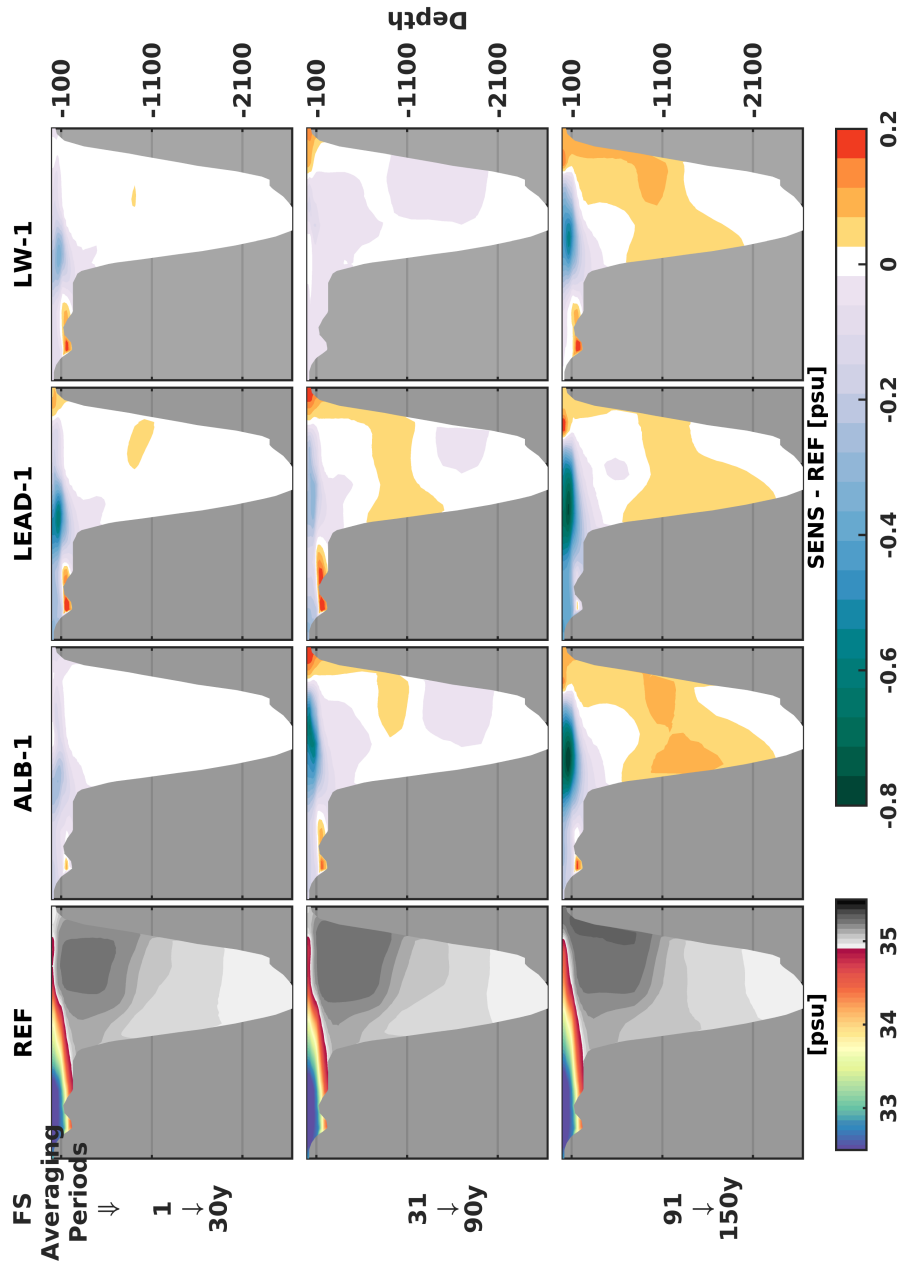


Figure 3.14: Salinity across Fram Strait section. From top to bottom: Ini30 (1 - 30y), Interm60 (31 - 90y) and Last60 (91 - 150y). Column I: Absolute values for REF run. Columns II - IV: difference maps between SENS-1 and REF as indicated.

3.3.2.2 Barents Sea: Volume and Heat Transport into the Arctic

The Barents Sea region is by far the most affected in all the experiments: sea ice concentration strongly reduces in all seasons, turbulent heat fluxes substantially increase from ocean to atmosphere, annually average TSURF rise up to 1.5°C and over Last60 period annual absolute averaged values slightly overcome the 0°C threshold.

In this work it is suggested that a compensation of the anomalous increased outflow through FS establishes through an increased volume flux into the Barents Sea (table 3.4). Thereafter, the investigation of the response and dynamical adjustment of the Barents Sea circulation system is done. To support this, changes in heat and volume flux across the section BSE, NBS, KG and BSX are discussed; keeping in mind, the terms inflow and outflow always refer to the interior and exterior of the Barents Sea, respectively. Figure 3.15 summarizes the Last60 average values of ocean volume and heat fluxes through Barents Sea sections and ocean-atmosphere heat turbulent and net heat flux.

Table 3.4: Averaged net Volume Flux changes through Barents Sea Entrance section. REF: absolute values are positive directed to the south. SENS values denote difference between averages (SENS - REF).

Year	1 – 30y	31 – 90y	91 – 150y
REF	2.54 ± 0.89	2.73 ± 0.93	3.22 ± 0.92
ALB-1	-0.03	0.43	0.57
LW-1	+0.03	0.27	0.42
LEAD-1	0.08	0.32	0.67

Barents Sea Entrance (BSE)

This section is defined from the north of Norway to the south of Svalbard, and is named Barents Sea Entrance (BSE). Net volume flux calculated in REF simulation overestimate somewhat the 2Sv pointed out in a review by [Beszczynska-Möller et al. \(2011\)](#). In REF the average net volume flux increases from 2.54 ± 0.89 Sv in Ini30 to 3.22 ± 0.92 during Last60. SENS net volume flux averages are comparable to REF in Ini30, however the increase related to Last60 overwhelms the increase in REF. How SENS

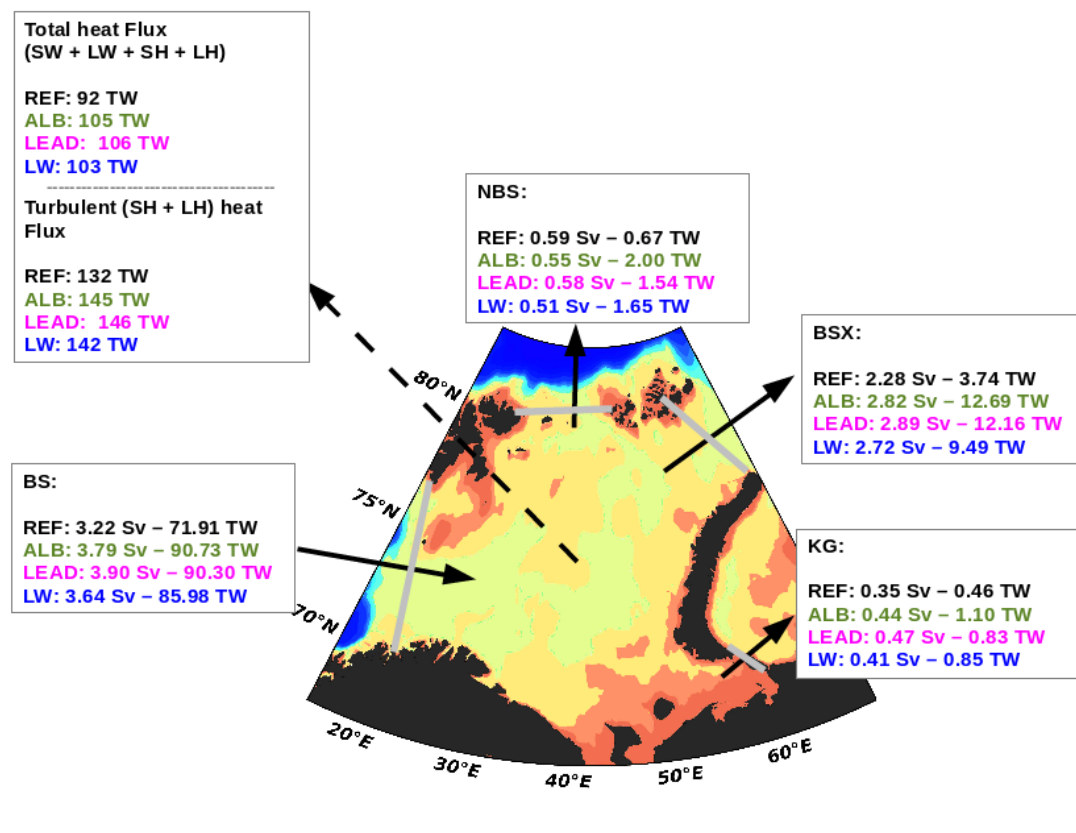


Figure 3.15: Last60 average volume and heat fluxes through Barents Sea sections. Solid arrows show direction of net volume flux across sections BSE, NBS, BSX and KG. Dashed arrow shows ocean-atmosphere turbulent and net heat flux averages for the area within 68 – 81°N and 17 – 67.5°E.

experiments differ from REF is shown in Table 3.4. The increased net volume flux outcomes from the combined effect of an increased inflow and a substantial decreased outflow.

The Bear Trench outflow together with Arctic waters carry initially (Ini30) ca. 0.8 Sv out of BSE section in REF and SENS simulations. In REF simulation average outflow reduces to almost half (0.45 ± 0.31), and in all SENS runs the average drops by half over the reduce REF value⁸. This suggests the outflow through the BS is a very vulnerable branch of local circulation to a changing Arctic, and is reasonably compromised under an increased sea ice melting scenario. The increase of AW into the Barents Sea at the expense of Arctic Water circulation has been observed and described in the work by Lind and Ingvaldsen (2012).

⁸See Table C.1 for mean values and corresponding uncertainties.

Heat flux averages for Ini30 period compare well in all experiments with recent estimates of 60 TW from high resolution model (Koenigk et al., 2012), and 70 TW from observed data Beszczynska-Möller et al. (2011) (Table C.2). The bulk of water entering the Barents Sea is on average up to 1°C warmer in all SENS compared to REF (with maximum differences up to 3°C). And, even though changes in the heat flux may be equally caused by modified water temperatures or velocity, in our simulations the changes between SENS and REF simulations are much larger for heat flux (up to 20 TW) than for the volume flux (on average 0.5 Sv, see Table 3.4), suggesting that mainly temperature raise is driving increased heat inflow.

Northern Barents Sea (NBS) and Kara Gate (KG)

The net volume inflow and outflow through NBS section stay rather constant in all simulations (REF and SENS), and have all a comparable net volume flux throughout the 150 years (from 0.5 to 0.6 Sv). However, a major change in heat fluxes gradually takes place. A consistent warming of water masses flowing both into and out of the Barents Sea is noticeable. The reason to this is again sustained by the warming of AW previously mentioned.

Moreover, warmer WSC flowing through FS section (discussed in section 3.3.2.1) feed the return flow entering the Barents Sea through the NBS (see Figure 1.5). The integrated volume outflow outweighs the inflow. In Ini30 and Intem60 it carries modified waters with temperature around 0°C out of the Barents Sea, and thus acts as a sink of heat to the Arctic Ocean. However, as waters in the Barents Sea warm, the outflow through the NBS exports water warmer than 0°C. Hence, it is converted into a source of heat to the Arctic Ocean. This trend is simulated in all experiments, but changes in SENS overwhelm those in REF.

Through KG, net volume transport is somewhat larger in SENS runs than in REF already in Ini30. The increased volume and temperature of AW flowing through BS is the fundamental reason for the hefty increase of net heat transport changes, along with the gradual increase of water net export.

Barents Sea Exit (BSX)

BSX section is the main export path of volume and heat out of the Barents Sea. Our REF run simulates an average net volume flux through the BSX of 1.77 ± 0.67 in Ini30. This value agrees reasonably well with the values ranging from 1.5 to 2.0 review in [Beszczynska-Möller et al. \(2011\)](#). A net volume flux increase trend is driven by a speed up of the outflow in all experiments (REF and SENS). In all SENS simulations, net volume flux out of the Barents Sea in Last60 is on average 0.53 Sv larger than in REF (2.28 Sv).

Most of the water leaving the Barents Sea through the BSX has been cooled down to temperature below 0°C ([Schauer et al., 2008](#)). Average values for Ini30 period are in agreement with the later statement, and the export of water masses with temperature lower than T_{ref} suggests the outflow is a source of heat to the basin. A substantial change of sign of net heat export is caused by the warmer AW inflow. Even though, the exceeding heat flux into the BS drives increased average turbulent heat fluxes (Table 3.2) from the ocean to the atmosphere, waters are not cooled to temperatures lower than 0°C . Consequently, the average net volume flux increase in the order of 0.53 Sv between SENS and REF is related to overriding heat export differences of ca. 9 TW in all SENS simulations.

The warmer outflow through BSX is in contrast to the finding by [Itkin et al. \(2014\)](#), where modelling of weaker sea ice simulated a cooling through St. Anna Trough of up to -0.45°C . In our work differences of outflow temperature between SENS and REF are larger or equal to 1°C on surface, and larger or equal to 0.5°C over bottom.

Changes in the cooling and mixing of AW in the Barents Sea can impact the ventilation of the AWL by altering the production of BSW. Figure 3.16 shows the average density of ocean water between the upper meters of the AWL, *i.e.* 230 and 680 m. In our simulations, AW temperature is leading the density differences in the BS. Positive thermal anomalies create a reverse change in density up to the central Barents Sea. Towards the St. Anna Trough, however, an opposite change in density is observed.

[Oziel et al. \(2015\)](#) suggest that an increased inflow of AW into the Barents Sea would lead to more outflow of BSW due to the feedback of local melting and freezing of sea ice. On the contrary, [Rudels et al. \(2013\)](#) states that under a regime of stronger AW

inflow no cooling to freezing temperatures occurs and no brine-induced convection to the bottom is possible, and density changes of the BSW outflow would be related to advected characteristics of the water mass.

It is suggested in this work that AW salinity positive anomalies advected across the Fram Strait and into the BS are potentially a major driver of these positive density anomalies. A thorough understanding of the exact mechanisms behind changes in our simulations is, however, not presented here.

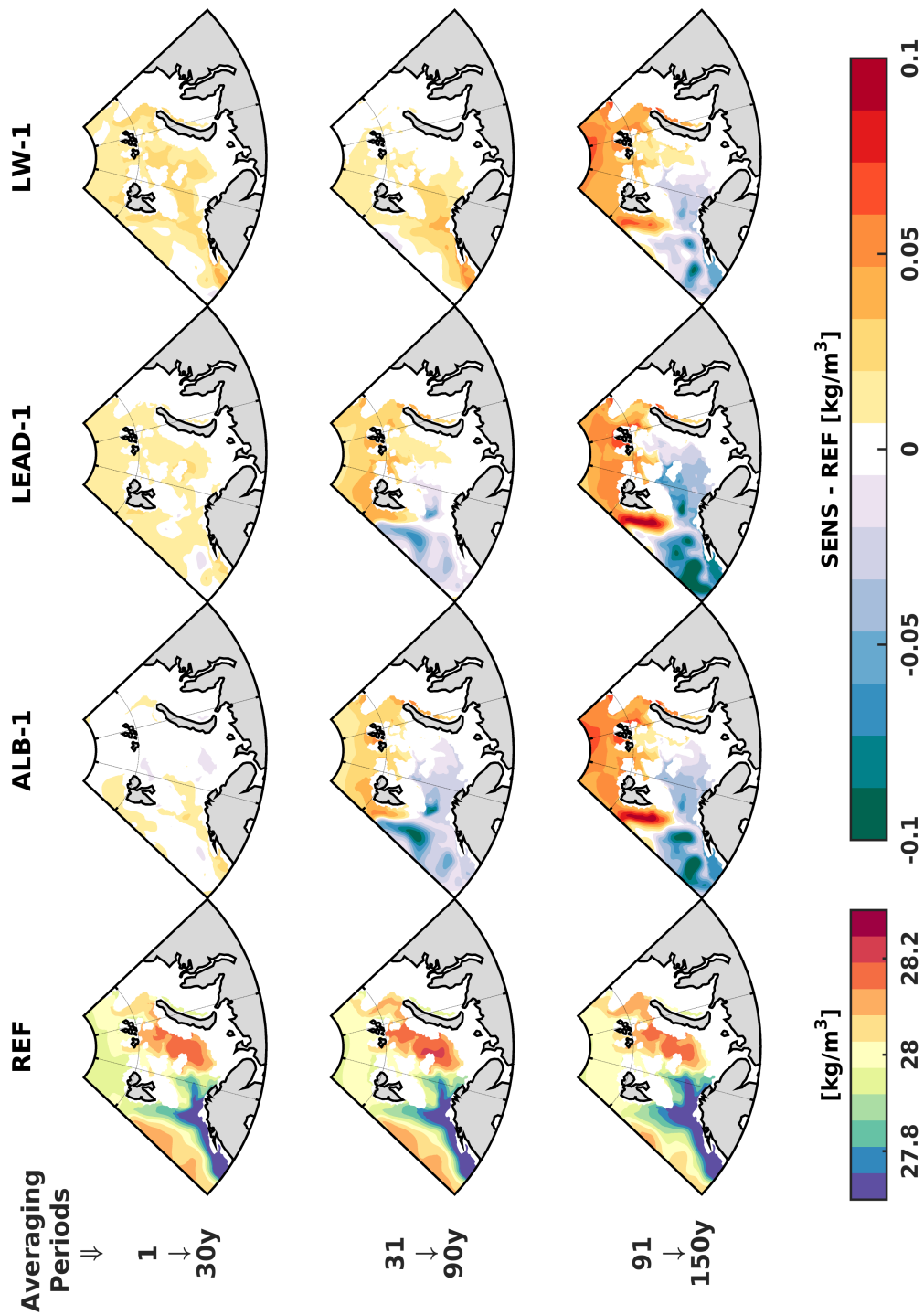


Figure 3.16: Average 230 – 680m density in the Barents Sea. From top to bottom: Ini30 (1 – 30y), Interm60 (31 – 90y) and Last60 (91 – 150y). Column I: Absolute values for REF run. Columns II - IV: difference maps between SENS-1 and REF as indicated.

Chapter 4

Summary and Outlook

4.1 Summary

This comparative study was concerned with addressing the changes in ocean circulation as a response to the gradual loss of Arctic sea ice. Sea ice retraction is forced by different physical perturbations in three sensitivity experiments (SENS). The ocean response in each SENS is evaluated against a common reference run (REF).

The overall state of REF compares fairly well with observations of the real system, but it is noteworthy to recall that the sensitivity simulations are idealized experiments, and should not be mistaken as predictions for future climate.

While in all SENS experiments fairly distinct sea ice area (SIA) changes are simulated, a steep sea ice volume (SIV) reduction occurs promptly after the introduction of each perturbation. The retraction of SIV is mostly driven by thinning of the ice all year round.

The reduced sea ice plays a particularly important role in areas formerly covered by more sea ice (area and thickness). Latent and sensible heat fluxes are increased mainly in the Barents Sea region and over the Greenland-Iceland-Norwegian (GIN) Seas. The latter differences agree with increased near-surface air temperature. No consistent changes in wind speed and mean sea level pressure are observed between such long time scale experiments.

For all three the physical perturbation comparable responses in the ocean are observed. All SENS simulations create a more mobile ice. As a consequence, larger momentum transfer may occur (between atmosphere-sea ice, atmosphere-ocean and ocean-sea ice). In turn, this mechanism causes the enhancement of the Beaufort Gyre and Transpolar Drift. As a consequence, increased net volume export of upper Arctic surface water is simulated through the Fram Strait (FS).

A compensation of the increased outflow through FS is evident across the Barents Sea Entrance (BSE) section. The enhancement of volume flux partly occurs at expense of the reduced outflow of the Bear Trench current. Also, it is shown in this work that the inflow and circulation of Arctic Water in the Barents Sea also lessens in a regime of increased AW inflow. In turn, the increased inflow into the Barents Sea is largely compensated by the outflow through the BSX section in all SENS. Notwithstanding, the input of heat into the Arctic is increased through all the passages (NBS, KG and BSX) in all SENS.

Along with increased volume flux into the Barents Sea, a substantial warming of the AW arises in all SENS experiments. A similar trend also occurs in the West Spitsbergen Current (WSC); it is argued that the positive anomalies carried by the different AW branches originate upstream and are consequence of the shift of the North Atlantic Current pathway. Also, salinity of AW inflow has increased.

The summation of increased volume and heat fluxes may impact the production of dense Barents Sea Water (BSW), which substantially fills the intermediate layer of the Arctic Ocean and eventually contribute to the deep branch of the Atlantic Meridional Overturning Circulation.

It was found that water being exported through the section Barents Sea Exit (BSX) is denser. The signal is fairly spread to the east and west of the St. Anna Trough and is substantial in the WSC inflow region. Therefore, it is hypothesized that these changes can be related to the increased salinity of the AW. Still, the understanding of the exact mechanisms behind this result need further assessment.

All in all, we believe that from this study it is possible to elucidate some ocean responses to the reduction of sea ice volume. Our SENS experiments suggest that on a centennial time scale the decrease of sea ice volume triggers an increased inflow of AW

into the Arctic Ocean, and potentially gives rise to modifications in the intermediate Arctic layer of Atlantic Water..

4.2 Outlook

The work conducted in this thesis contributes to the increasing effort of addressing the implications of Arctic sea ice decline on the oceanic circulation. Although some relevant results were described and investigated, many questions remain open.

The leading role of the ocean component on the development of long time scales anomalies is a clear message from our results. However, the exact mechanism behind this remains uncertain in the particular case of this study. A detailed investigation of the results for the North Atlantic ocean circulation is beyond the scope of the present study. Notwithstanding, the verification of the impact of sea ice reduction on the subpolar gyre and overall circulation structure can provide important insight into the nature of coupled interactions on long time scales.

Due to time limitations, the quantitative assessment of sea ice export has not been done. The results presented in this study would strongly benefit of a more detailed verification of sea ice export.

For addressing the strongly linked sea ice-ocean system in the Barents Sea region, a better representation of hydrography and, consequently, a more realistic sea ice coverage could be achieved by running the simulations at higher resolutions. Previous studies show that including a more accurate representation of the topography and resolving a larger number of small scale features (*e.g.* sea ice fractures, mesoscale dynamics) is particularly important for representing the local and regional climate.

Appendix A

Glossary

- **Albedo:** Albedo (from the Latin *albus* for "white") is the fraction of light that is reflected by a body or surface.

Planetary Albedo: a measure of the combined atmospheric and surface reflectivity

- **Autotrophic:** Autotroph. Organism capable of synthesizing energy-containing organic molecules from inorganic substances using light or chemical energy.
- **Sea ice concentration:** Fraction of cell area covered by sea ice ranging from 0 to 1 (0 to 100%).
- **Sea ice area:** Concentration/fraction of sea ice multiplied by each grid cell area. Parameter takes sea ice fractures into account.
- **Sea ice extent:** Maximum reach of sea ice cover, disregarding discontinuities (fractures) of the layer.
- **Sea ice volume:** Area of sea ice relative to each cell multiplied by its thickness.
- **Physical and Biological uptake:** Physical uptake of CO₂ driven by increased solubility due to ocean water cooling, mixing and turbulence at surface. Biological uptake configures as the drawdown of CO₂ by photosynthetic organisms.

Appendix B

Figures

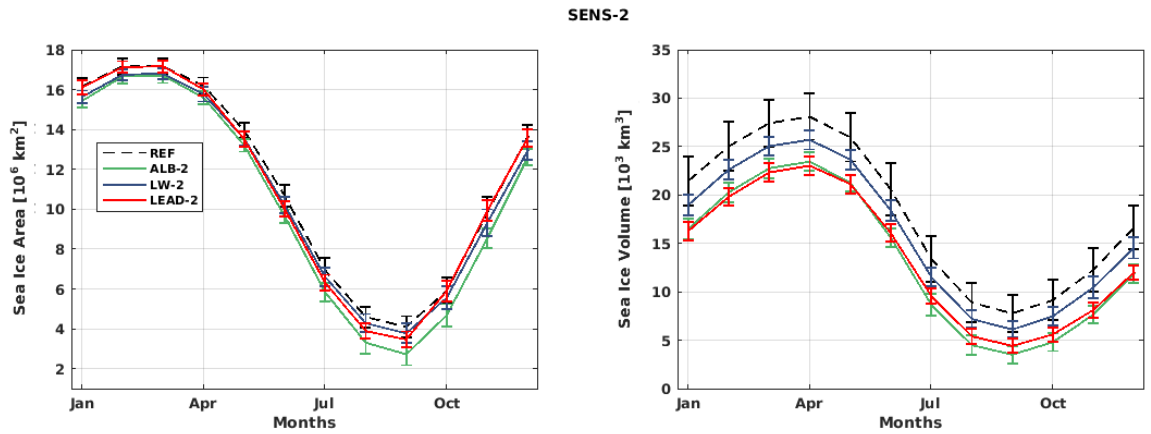


Figure B.1: SENS-2 development within Ini30 of SIA and SIV as climatological monthly means, with error bars associated with year-to-year standard deviation

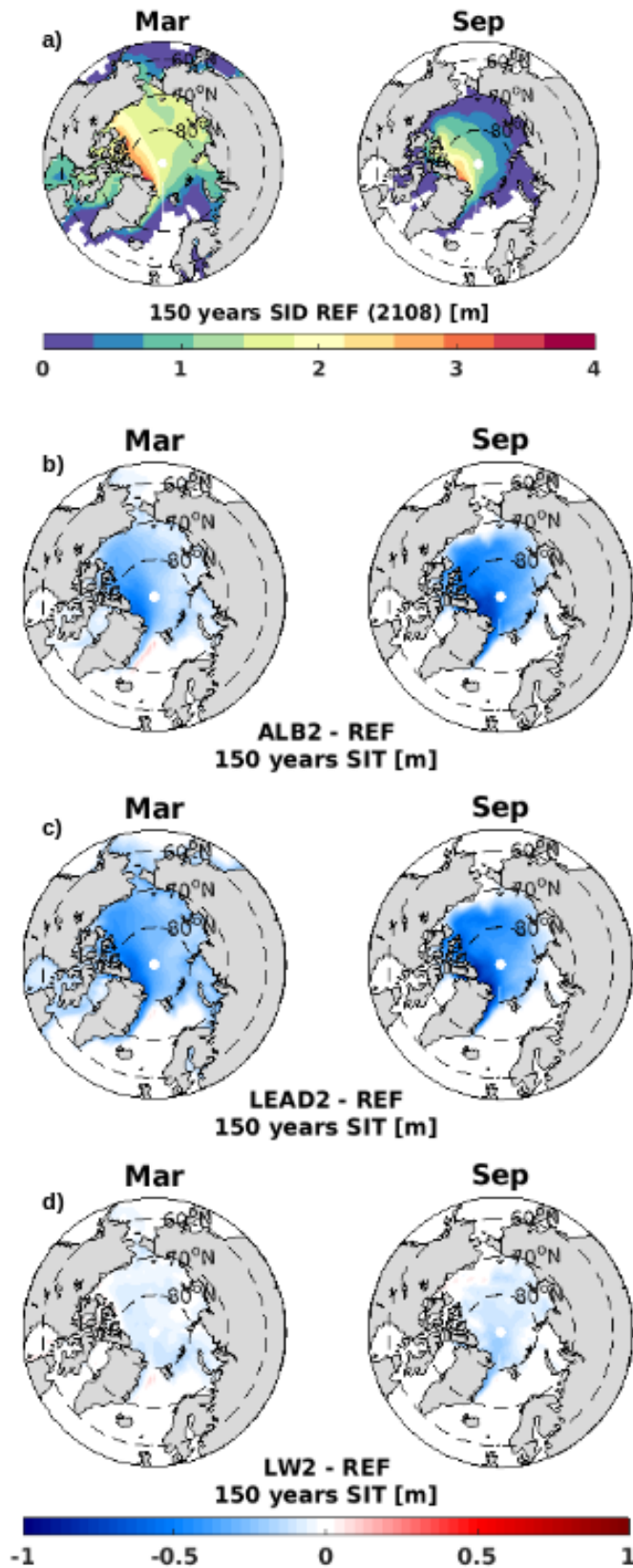


Figure B.2: Sea ice thickness: 150 year absolute values (REF) and difference maps (SENS-2 - REF). (2108) indicating averaging period from year 70 to year 220 after experiment initialization.

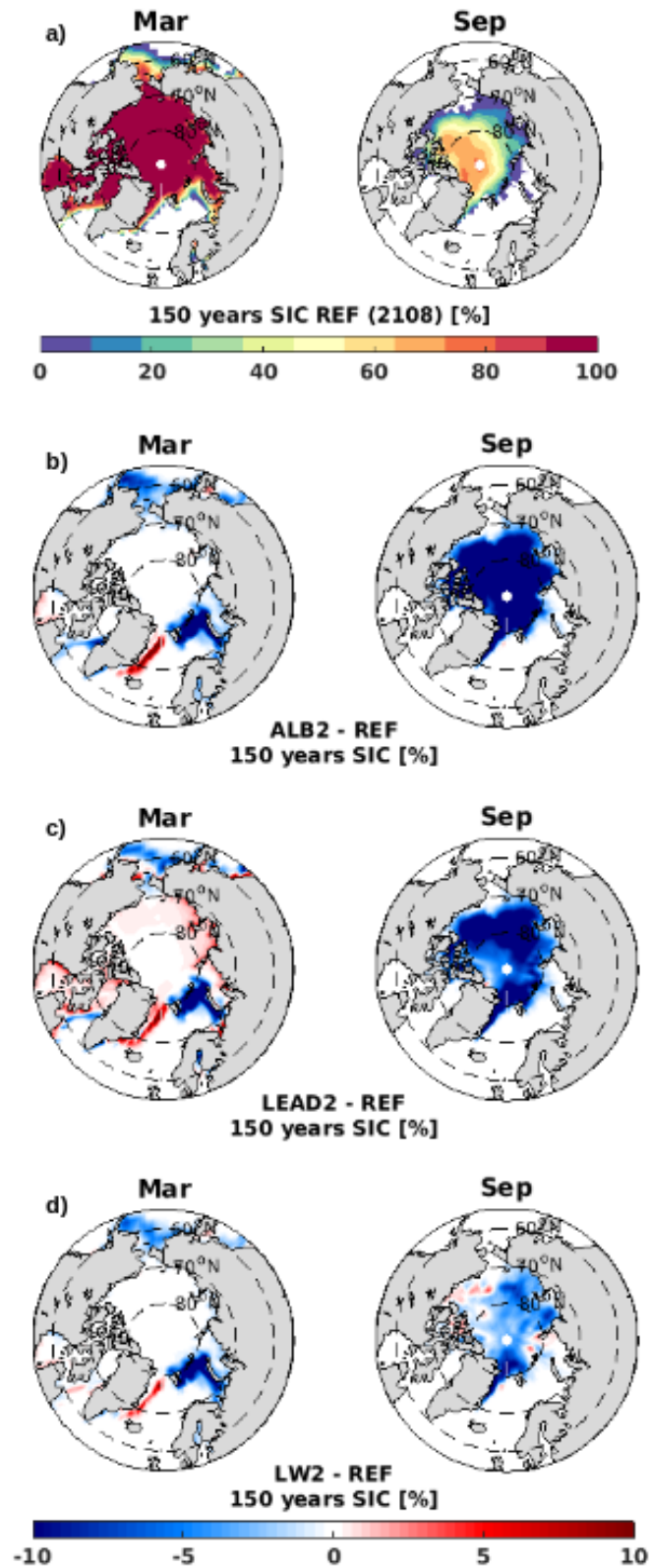


Figure B.3: Sea ice concentration (SIC): 150 year absolute average (REF) and difference maps (SENS-2 - REF). (2108) indicating averaging period from year 70 to year 220 after experiment initialization.

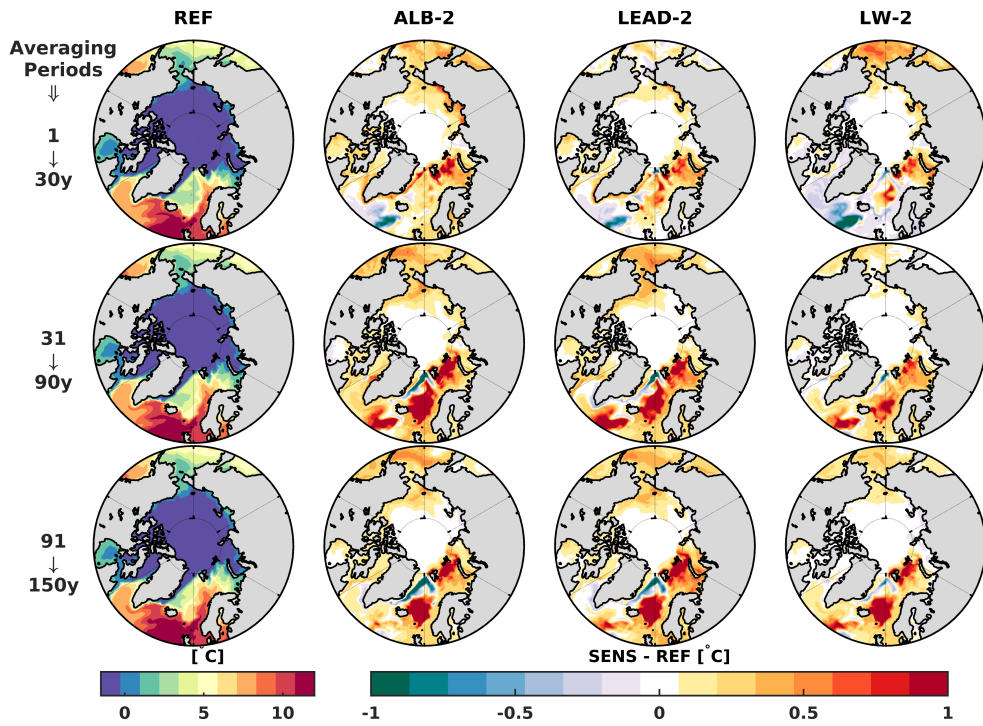


Figure B.4: Average SST north of 55° N. From top to bottom: Ini30 (1 – 30y), Interm60 (31 – 90y) and Last60 (91 – 150y). Column I: Absolute values for REF run. Columns II - IV: difference maps between SENS-2 and REF as indicated.

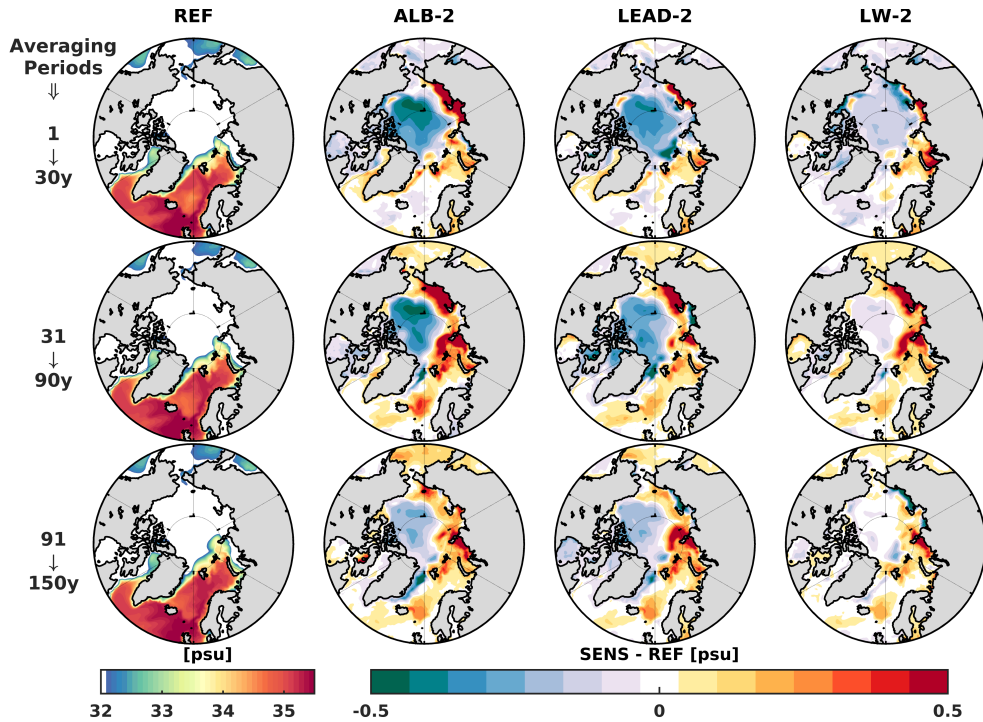


Figure B.5: Average SSS north of 55° N. From top to bottom: Ini30 (1 – 30y), Interm60 (31 – 90y) and Last60 (91 – 150y). Column I: Absolute values for REF run. Columns II - IV: difference maps between SENS-2 and REF as indicated

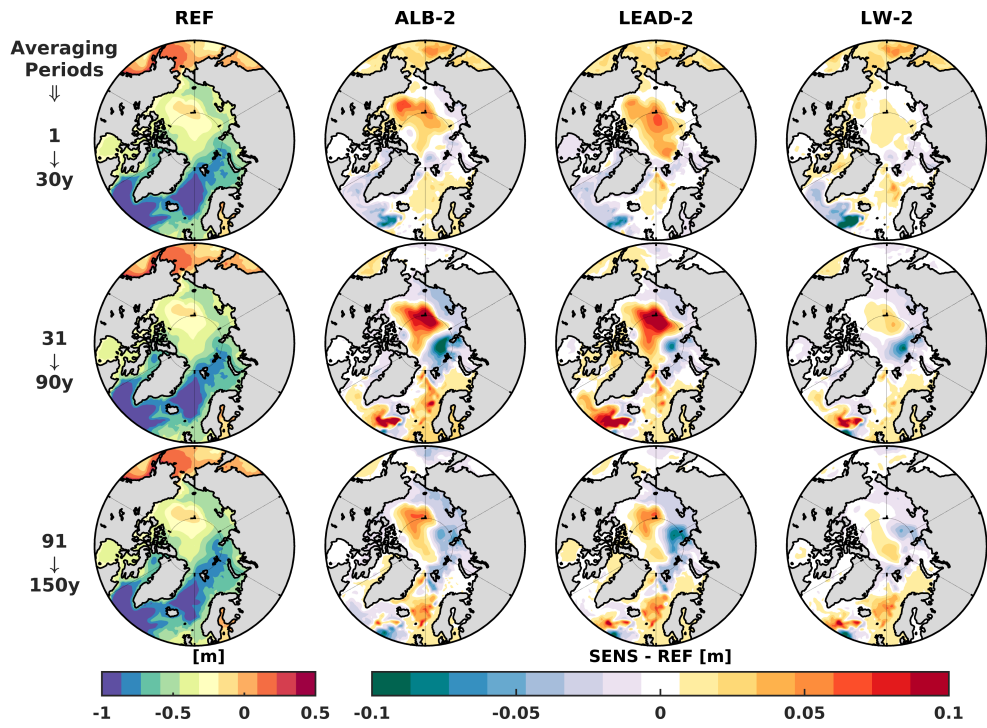


Figure B.6: Average SSH north of 55° N. From top to bottom: Ini30 (1 – 30y), Interm60 (31 – 90y) and Last60 (91 – 150y). Column I: Absolute values for REF run. Columns II - IV: difference maps between SENS-2 and REF as indicated

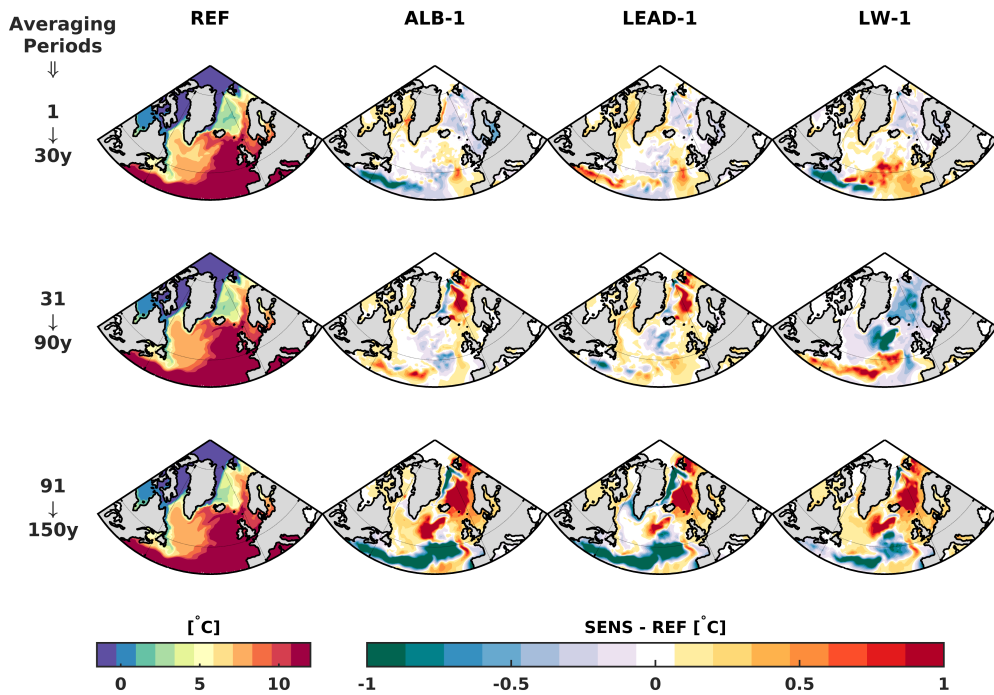


Figure B.7: North Atlantic (north of 40° N) average 0 - 50 m ocean temperature maps. From top to bottom: Ini30 (1 – 30y), Interm60 (31 – 90y) and Last60 (91 – 150y). Column I: Absolute values for REF run. Columns II - IV: difference plots between SENS-1 and REF as indicated

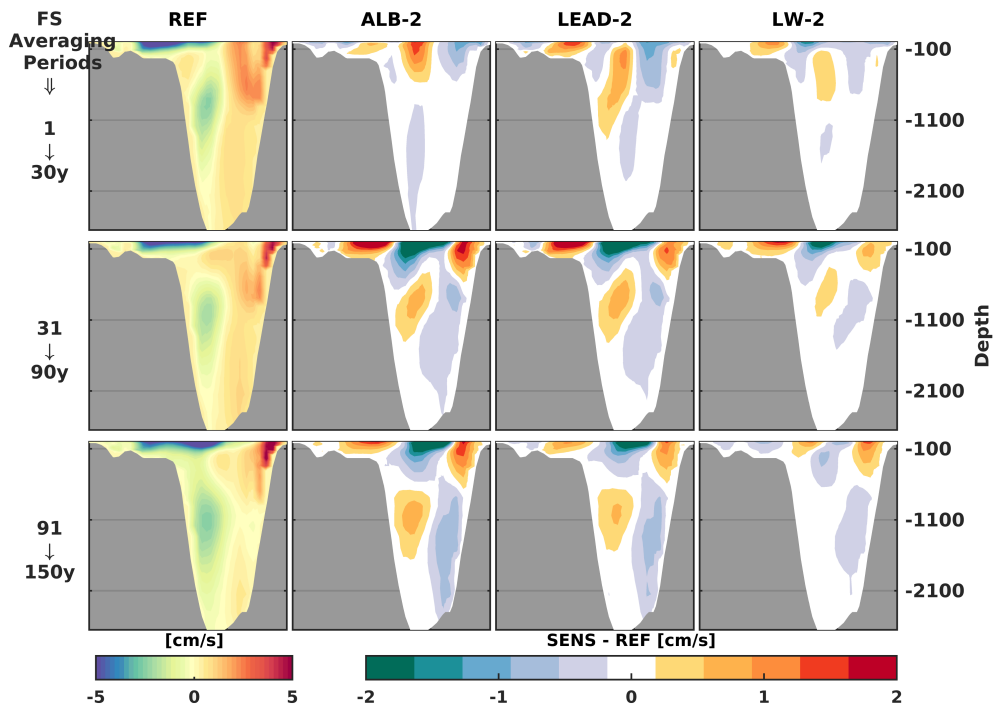


Figure B.8: Velocity across Fram Strait section. From top to bottom: Ini30 (1 – 30y), Interm60 (31 – 90y) and Last60 (91 – 150y). Column I: Absolute values for REF run. Columns II - IV: difference maps between SENS-2 and REF as indicated.

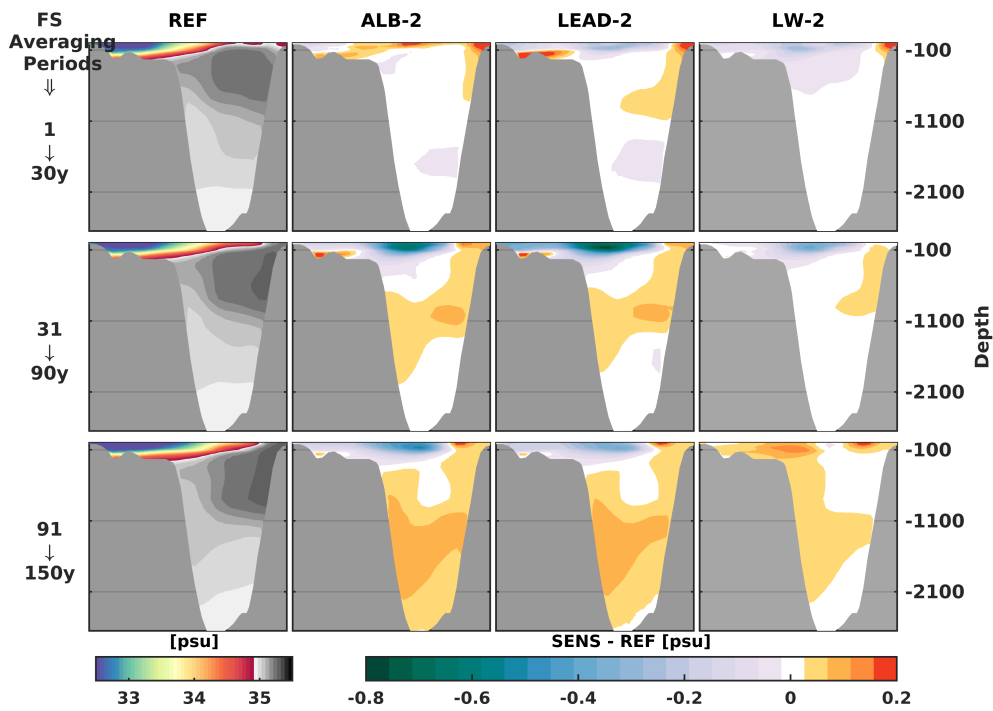


Figure B.9: Salinity across Fram Strait section. From top to bottom: Ini30 (1 – 30y), Interm60 (31 – 90y) and Last60 (91 – 150y). Column I: Absolute values for REF run. Columns II - IV: difference maps between SENS-2 and REF as indicated.

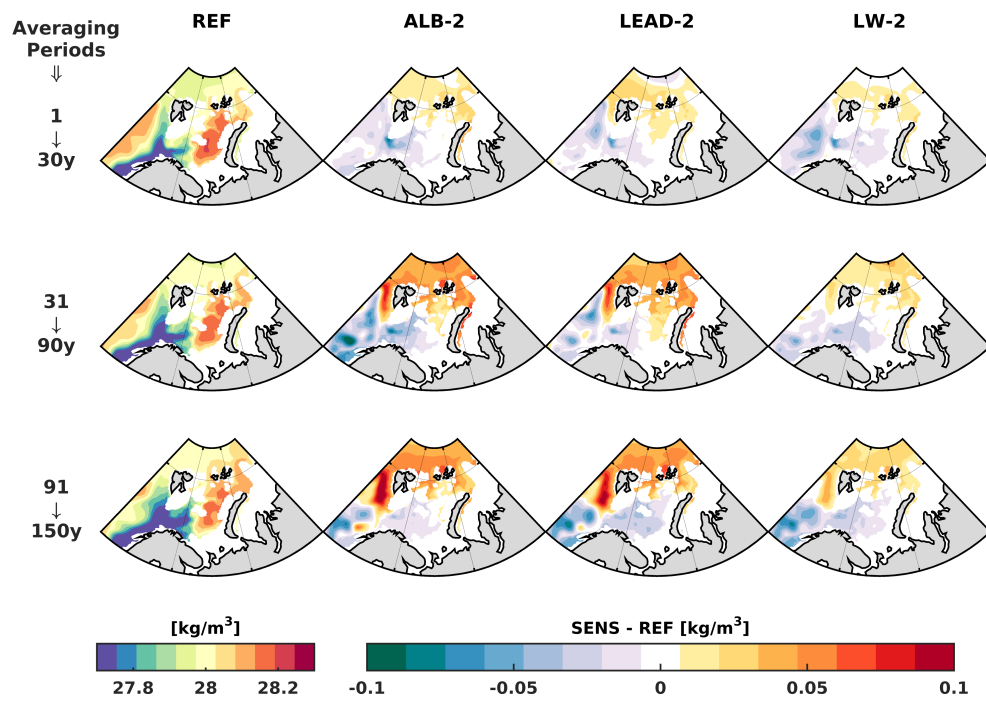


Figure B.10: Average 230 – 680m density in the Barents Sea. From top to bottom: Ini30 (1 – 30y), Interm60 (31 – 90y) and Last60 (91 – 150y). Column I: Absolute values for REF run. Columns II - IV: difference maps between SENS-2 and REF as indicated.

Appendix C

Tables

Table C.2: Averaged ocean heat flux through BSE section

Avg.Period	[TW]	BSE			
		REF	ALB-1	LEAD-1	LW-1
1 - 30	Inflow	64.80 ± 19.45	62.58 ± 18.93	64.29 ± 17.73	63.37 ± 17.30
	Outflow	-10.03 ± 5.25	-9.58 ± 5.18	-9.51 ± 4.82	-9.77 ± 5.28
	Net	54.76 ± 18.98	53.00 ± 18.43	54.78 ± 18.17	53.59 ± 17.38
31 - 90	Inflow	70.66 ± 19.85	76.63 ± 20.68	74.74 ± 21.13	73.73 ± 21.27
	Outflow	-10.84 ± 5.79	-7.64 ± 5.37	-8.57 ± 5.96	-8.57 ± 5.57
	Net	59.82 ± 20.02	68.98 ± 21.71	66.17 ± 22.39	65.16 ± 22.48
91 - 150	Inflow	79.94 ± 20.14	95.33 ± 23.99	93.63 ± 22.56	91.56 ± 22.00
	Outflow	-8.03 ± 5.61	-4.60 ± 4.32	-5.58 ± 5.30	-3.32 ± 3.08
	Net	71.91 ± 21.47	90.73 ± 25.19	90.30 ± 23.40	85.98 ± 23.30

Table C.1: Volume Flux across FS and BSE sections. Inflow and outflow always referenced to the Arctic Ocean

Avg.Period	[Sv]	FS					BSE				
		REF	ALB-1	LEAD-1	LW-1	REF	ALB-1	LEAD-1	LW-1		
1 - 30	Inflow	3.45 ± 1.38	3.36 ± 1.49	2.94 ± 1.30	2.98 ± 1.28	3.37 ± 0.76 ±	3.37 ± 0.80	3.40 ± 0.74	3.39 ± 0.75		
	Outflow	-5.77 ± 1.57	-5.66 ± 1.65	-5.31 ± 1.48	-5.23 ± 1.62	-0.83 ± 0.36	-0.85 ± 0.37	-0.78 ± 0.31	-0.81 ± 0.36		
	Net	-2.32 ± 0.80	-2.31 ± 0.83	-2.36 ± 0.79	-2.25 ± 0.84	2.54 ± 0.89	2.51 ± 0.90	2.62 ± 0.87	2.57 ± 0.87		
31 - 90	Inflow	3.09 ± 1.25	2.53 ± 0.88	2.72 ± 0.93	2.82 ± 1.00	3.51 ± 0.79	3.63 ± 0.78	3.59 ± 0.84	3.56 ± 0.83		
	Outflow	-5.51 ± 1.44	-5.38 ± 1.39	-5.49 ± 1.37	-5.51 ± 1.47	-0.78 ± 0.37	-0.46 ± 0.31	-0.54 ± 0.35	-0.56 ± 0.35		
	Net	-2.43 ± 0.84	-2.85 ± 0.91	-2.77 ± 0.93	-2.68 ± 0.92	2.73 ± 0.93	3.17 ± 0.91	3.05 ± 0.99	3.00 ± 0.96		
91 - 150	Inflow	2.71 ± 0.94	2.62 ± 0.84	2.51 ± 0.76	2.58 ± 0.81	3.67 ± 0.79	4.02 ± 0.87	4.10 ± 0.90	3.92 ± 0.85		
	Outflow	-5.59 ± 1.33	-6.29 ± 1.29	-6.47 ± 1.29	-5.89 ± 1.33	-0.45 ± 0.31	-0.23 ± 0.21	-0.17 ± 0.15	-0.28 ± 0.25		
	Net	-2.88 ± 0.89	-3.66 ± 0.95	-3.96 ± 0.94	-3.32 ± 0.93	3.22 ± 0.92	3.79 ± 0.95	3.90 ± 0.95	3.64 ± 0.94		

Table C.3: Net spatial average Turbulent and Net Heat Flux over Barents Sea. Results from **SENS-2**

Avg.Period [TW]		BSE			
		REF	ALB-2	LEAD-2	LW-2
1 - 30	TH ↑	115	122	121	120
	NET ↓	77	80	81	79
31 - 90	TH ↑	126	140	137	133
	NET ↓	87	101	97	93
91 - 150	TH ↑	138	147	149	146
	NET ↓	99	108	110	103

TH: Turbulent Heat = SH + LH
NET: SW + LW + SH + LH
↑ : from ocean to atmosphere
↓ : from atmosphere to ocean

Bibliography

- Aagaard, K. and Carmack, E. C. (1989). The role of sea ice and other fresh water in the Arctic circulation. *Journal of Geophysical Research*, 94(C10):14485.
- Årthun, M., Eldevik, T., Smedsrud, L. H., Skagseth, O., and Ingvaldsen, R. B. (2012). Quantifying the Influence of Atlantic Heat on Barents Sea Ice Variability and Retreat*. *Journal of Climate*, 25(13):4736–4743.
- Bader, J., Mesquita, M. D., Hodges, K. I., Keenlyside, N., Østerhus, S., and Miles, M. (2011). A review on Northern Hemisphere sea-ice, storminess and the North Atlantic Oscillation: Observations and projected changes. *Atmospheric Research*, 101(4):809–834.
- Beszczynska-Möller, A., Woodgate, R., Lee, C., Melling, H., and Karcher, M. (2011). A Synthesis of Exchanges Through the Main Oceanic Gateways to the Arctic Ocean. *Oceanography*, 24(3):82–99.
- Budikova, D. (2009). Role of Arctic sea ice in global atmospheric circulation: A review. *Global and Planetary Change*, 68(3):149–163.
- Carmack, E., Polyakov, I., Padman, L., Fer, I., Hunke, E., Hutchings, J., Jackson, J., Kelley, D., Kwok, R., Layton, C., Melling, H., Perovich, D., Persson, O., Ruddick, B., Timmermans, M.-L., Toole, J., Ross, T., Vavrus, S., and Winsor, P. (2015). TOWARDS QUANTIFYING THE INCREASING ROLE OF OCEANIC HEAT IN SEA ICE LOSS IN THE NEW ARCTIC. *Bulletin of the American Meteorological Society*, page 150203142711003.
- Cavalieri, D. J. and Parkinson, C. L. (2012). Arctic sea ice variability and trends, 1979–2010. *The Cryosphere*, 6(4):881–889.
- Deser, C., Tomas, R. A., and Sun, L. (2015). The Role of Ocean-Atmosphere Coupling in the Zonal-Mean Atmospheric Response to Arctic Sea Ice Loss. *Journal of Climate*, 28(6):2168–2186.
- Holliday, N. P., Hughes, S. L., Bacon, S., Beszczynska-Möller, A., Hansen, B., Lavín, A., Loeng, H., Mork, K. A., Østerhus, S., Sherwin, T., and Walczowski, W. (2008). Reversal of the 1960s to 1990s freshening trend in the northeast North Atlantic and Nordic Seas. *Geophysical Research Letters*, 35(3):L03614.
- IPCC (2007). Technical Summary. In *Climate Change 2007: The Physical Science Basis. Contribution of Working Group I to the Fourth Assessment Report of the Intergovernmental Panel on Climate Change*. Cambridge University Press, Cambridge, United Kingdom and New York, NY, USA.

- IPCC (2013). Technical Summary. In *Climate Change 2013: The Physical Science Basis. Contribution of Working Group I to the Fifth Assessment Report of the Intergovernmental Panel on Climate Change*. Cambridge University Press, Cambridge, United Kingdom and New York, NY, USA.
- Itkin, P., Karcher, M., and Gerdes, R. (2014). Is weaker Arctic sea ice changing the Atlantic water circulation? *Journal of Geophysical Research: Oceans*, 119(9):5992–6009.
- Koenigk, T. and Brodeau, L. (2013). Ocean heat transport into the Arctic in the twentieth and twenty-first century in EC-Earth. *Climate Dynamics*, 42(11-12):3101–3120.
- Koenigk, T., Brodeau, L., Graverson, R. G., Karlsson, J., Svensson, G., Tjernström, M., Willén, U., and Wyser, K. (2012). Arctic climate change in 21st century CMIP5 simulations with EC-Earth. *Climate Dynamics*, 40(11-12):2719–2743.
- Kwok, R., Cunningham, G. F., Wensnahan, M., Rigor, I., Zwally, H. J., and Yi, D. (2009). Thinning and volume loss of the Arctic Ocean sea ice cover: 2003–2008. *Journal of Geophysical Research*, 114(C7):C07005.
- Lind, S. and Ingvaldsen, R. B. (2012). Variability and impacts of Atlantic Water entering the Barents Sea from the north. *Deep Sea Research Part I: Oceanographic Research Papers*, 62:70–88.
- Mauritzen, C., Rudels, B., and Toole, J. (2013). *Ocean Circulation and Climate - A 21st Century Perspective*, volume 103 of *International Geophysics*. Elsevier, 2 edition.
- NSIDC (2014). National Snow And Ice Data Center: All about sea ice. [url:http://nsidc.org/seaice/](http://nsidc.org/seaice/).
- Oziel, L., Sirven, J., and Gascard, J.-C. (2015). The Barents Sea polar front and water masses variability (1980–2011). *Ocean Science Discussions*, 12(2):449–492.
- Parkinson, C. L. and Comiso, J. C. (2013). On the 2012 record low Arctic sea ice cover: Combined impact of preconditioning and an August storm. *Geophysical Research Letters*, 40(7):1356–1361.
- Pistone, K., Eisenman, I., and Ramanathan, V. (2014). Observational determination of albedo decrease caused by vanishing Arctic sea ice. *Proceedings of the National Academy of Sciences of the United States of America*, 111(9):3322–6.
- Rudels, B., Schauer, U., Björk, G., Korhonen, M., Pisarev, S., Rabe, B., and Wisotzki, A. (2013). Observations of water masses and circulation with focus on the Eurasian Basin of the Arctic Ocean from the 1990s to the late 2000s. *Ocean Science*, 9(1):147–169.
- Schauer, U. and Beszczynska-Möller, A. (2009). Problems with estimation and interpretation of oceanic heat transport—conceptual remarks for the case of fram strait in the arctic ocean. *Ocean Science*, 5(4):487–494.
- Schauer, U., Beszczynska-Möller, A., Walczowski, W., Fahrbach, E., Piechura, J., and Hansen, E. (2008). Variation of Measured Heat Flow Through the Fram Strait Between 1997 and 2006. In *ArcticSubarctic Ocean Fluxes*, pages 65–85. Springer Netherlands, Dordrecht.
- Schauer, U., Loeng, H., Rudels, B., Ozhigin, V. K., and Dieck, W. (2002). Atlantic water flow through the barents and kara seas. *Deep Sea Research Part I: Oceanographic Research Papers*, 49(12):2281–2298.

- Semmler, T., McGrath, R., and Wang, S. (2012). The impact of Arctic sea ice on the Arctic energy budget and on the climate of the Northern mid-latitudes. *Climate Dynamics*, 39(11):2675–2694.
- Serreze, M. C. and Barry, R. G. (2011). Processes and impacts of Arctic amplification: A research synthesis. *Global and Planetary Change*, 77(1-2):85–96.
- Sidorenko, D., Rackow, T., Jung, T., Semmler, T., Barbi, D., Danilov, S., Dethloff, K., Dorn, W., Fieg, K., Goessling, H. F., Handorf, D., Harig, S., Hiller, W., Juricke, S., Losch, M., Schröter, J., Sein, D. V., and Wang, Q. (2014). Towards multi-resolution global climate modeling with ECHAM6FESOM. Part I: model formulation and mean climate. *Climate Dynamics*.
- Smedsrud, L. H., Esau, I., Ingvaldsen, R. B., Eldevik, T., Haugan, P. M., Li, C., Lien, V. S., Olsen, A., Omar, A. M., Otterå, O. H., Risebrobakken, B. r., Sandø, A. B., Semenov, V. A., and Sorokina, S. A. (2013). THE ROLE OF THE BARENTS SEA IN THE ARCTIC CLIMATE SYSTEM. *Reviews of Geophysics*, 51:415–449.
- Stevens, B., Giorgetta, M., Esch, M., Mauritsen, T., Crueger, T., Rast, S., Salzmann, M., Schmidt, H., Bader, J., Block, K., Brokopf, R., Fast, I., Kinne, S., Kornblueh, L., Lohmann, U., Pincus, R., Reichler, T., and Roeckner, E. (2013). Atmospheric component of the MPI-M Earth System Model: ECHAM6. *Journal of Advances in Modeling Earth Systems*, 5(2):146–172.
- Thomas, D. N. and Dieckmann, G. S. (2009). *Sea Ice*. Wiley-Blackwell, Oxford, UK.
- Tomczak, M. and Godfrey, J. S. (1994). *Regional Oceanography: an introduction*. Pergamon, Oxford, UK.
- Vihma, T. (2014). Effects of Arctic Sea Ice Decline on Weather and Climate: A Review. *Surveys in Geophysics*, 35(5):1175–1214.
- Walczowski, W. (2014). *Atlantic Water in the Nordic Seas*. GeoPlanet: Earth and Planetary Sciences. Springer International Publishing, Cham.
- Wang, Q., Danilov, S., Sidorenko, D., Timmermann, R., Wekerle, C., Wang, X., Jung, T., and Schröter, J. (2014). The Finite Element Sea Ice-Ocean Model (FESOM) v.1.4: formulation of an ocean general circulation model. *Geoscientific Model Development*, 7(2):663–693.
- Wilcoxon, F. (1946). Individual Comparisons by Ranking Methods. *Journal of Economic Entomology*, 39(6):80–83.
- Winton, M. (2008). *Arctic Sea Ice Decline: Observations, Projections, Mechanisms, and Implications*. Geophysical Monograph Series. American Geophysical Union, Washington, D.C.
- Zhang, J. and Rothrock, D. A. (2003). Modeling Global Sea Ice with a Thickness and Enthalpy Distribution Model in Generalized Curvilinear Coordinates. *Monthly Weather Review*, 131(5):845–861.
- Zickfeld, K., Levermann, A., Morgan, M. G., Kuhlbrodt, T., Rahmstorf, S., and Keith, D. W. (2007). Expert judgements on the response of the Atlantic meridional overturning circulation to climate change. *Climatic Change*, 82(3-4):235–265.